



UNIVERSITY COLLEGE LONDON (UCL)

ELEC0036

Oxygen Diamond Sensors for Extreme Environments

Author

MIRUNA-CRISTIANA
MORARU

Student Number

17016624

Supervisor

Prof R. JACKMAN

Second Supervisor

Prof J. MORTON

April 21, 2020
A BEng Project Final Report

Declaration of Originality

I have read and understood the College and Department's statements and guidelines concerning plagiarism.

I declare that all material described in this report is all my own work except where explicitly and individually indicated in the text. This includes ideas described in the text, figures and computer programs.

Name: Miruna-Cristiana Moraru

Date: 20.04.2020

Signature:



Abstract

This project examines the attributes of diamond technology for working electrodes within the design of an oxygen sensor for extreme environments. Three diamond-based experimental samples are considered, and their performance as working electrodes is evaluated. The three samples are a Pt-on-diamond microelectrode array (PtDMA), a Pt-on-BDD (PtBDD) electrode, and a Graphic Microchannel Array (GMC) electrode. Periodic cyclic voltammetry and chronoamperometry procedures are performed. The samples are in turns the working electrodes for an oxygen sensor setup. The results are interpreted, and part of the data is plotted in descriptive graphs for a thorough analysis. For the two samples with microchannel arrays, the change from Cottrellian behaviour for small-time values to steady-state diffusion-limited current was observed.

The relevant oxygen sensor metrics are determined in each of the three separate cases. Parameters such as the coefficient of correlation, response time and stability are identified and compared with those of oxygen sensors reported in several studies. This comparison shows that all three proposed electrodes have impressive characteristics and could be used to detect the concentration of oxygen sensitively. The PtBDD electrode has excellent long-term response stability with a current drift of less than 1.4% and a fast response time of 1s. The PtDMA and the GMC show better calibration curves, with the latter having a stronger reduction current correlation with the dissolved oxygen concentration ($R^2 = 0.999$, for an O_2 range 4-14.5 mg/l).

The GMC has been demonstrated for the first time as an electrode for oxygen sensors. It proved to have the highest accuracy of all three electrodes and performed well in every electrochemical experiment. Its detection limit and response time were also satisfactory, with values of 0.185mg/l, and 8.3s, respectively. A concept for an oxygen sensor with the GMC as its working electrode has been designed and presented.

Acknowledgements

I would like to express my sincere gratitude to my project supervisor Prof Richard Jackman for his invaluable and insightful feedback throughout this entire project. His great encouragements were always appreciated. In addition, I want to thank Dr Ralph J. Moors for providing the diamond samples used in this project, and for his guidance every step of the way. His willingness to share his time, as well as knowledge on oxygen sensors, was highly valued. My thanks are also extended to Dr Joe Welch for his support and assistance in holding my progress to date. Along with them, I further want to recognize the support and encouragement of all Diamond Electronics Ltd members.

I would also like to thank my family and friends for their love and comfort throughout this project, for which I will forever be grateful.

Contents

1	Introduction	6
2	Aims and Objectives	8
3	Theory and Analytical Bases for the Work	9
3.1	Carbon Materials	9
3.1.1	Diamond	10
3.1.1.1	Crystal Structure	10
3.1.1.2	Diamond Production	10
3.1.1.3	Properties of Diamond	11
3.1.1.4	Dopping of Diamond	12
3.1.2	sp ₂ Carbon	13
3.2	Oxygen Sensors	14
3.2.1	Iodometric Titration	14
3.2.2	Optical Sensing	15
3.2.3	The Electrochemical Detection and the Amperometric Oxygen Sensor	15
3.3	Principles of oxygen sensing	16
3.3.1	Dissolved Oxygen	16
3.3.2	The Oxygen Reduction Reaction (ORR)	17
3.3.3	Diffusion limited currents at various electrode geometries	17
3.3.3.1	Cottrell Plot	18
3.3.4	Microelectrodes	18
3.3.4.1	Mass Transport	19
3.3.4.2	Discrimination Against Charging Currents	20
3.3.4.3	Reduced Distortion from IR Drop	20
3.3.4.4	Reduced Area	21
3.4	Defining the extreme environment conditions in the context of the project	21
4	Technical Method	21
4.1	Electrochemical Measurements	21
4.1.1	Cyclic Voltammetry	22
4.1.2	Potential Step Voltammetry	23
4.1.3	Performance Indices of Oxygen Sensors	24
4.1.3.1	Stability over time and Current Drift	24
4.1.3.2	Response time	25
4.1.3.3	Linearity	25
4.1.3.4	Sensitivity	25
4.1.3.5	Accuracy Detection Limit	25
4.2	The Design of the Electrochemical Cell	25
4.3	The fabrication methods of the working electrodes	26
4.3.1	The Pt-on-diamond microelectrode array	26
4.3.2	The 3nm-Pt-on-BDD electrode	27
4.3.3	The Graphitic Microelectrode Array	27
5	Results	28

5.1	Pt-on-diamond microelectrode array (PtDMA)	28
5.2	3nm Pt NPs on BDD electrode (PtBDD)	32
5.3	Graphitic Microchannel Array (GMC)	37
5.4	Discussion	40
5.5	Design Concept	43
6	Conclusion	48

1 Introduction

This project aims to address features of the diamond technology for the design of an oxygen sensor for harsh environmental applications that can simultaneously perform all oxygen measurements in real-time, without the need for collecting samples. In particular, this project follows the study of three diamond-based working electrodes and their performance within an oxygen sensor.

In the past two decades, considerable efforts have been made to address environmental issues and concerns in research and technology development. For several years, the need to reduce carbon emissions from various industrial fields has led to an increase in academic research on gas sensors. Particularly, oxygen sensors had an essential role in monitoring emissions through automotive engine management, chemical process management, factory boiler control. Besides, the measurement of the dissolved oxygen (DO) concentration is considered one of the most relevant indicators for the aquatic health metrics. Fish, algae, and all other living marine organisms require a dissolved oxygen concentration of at least 8mg/L for survival [1]. If DO is reduced from the composition of water, the anaerobic bacteria increases excessively, leading to permanently damaged water systems. The DO concentration in the ocean is also an indicator of the production of phytoplankton, which is responsible for 80% of the world's oxygen. Therefore, their monitoring is especially crucial to climate scientists. The oxygen sensors available on the market possess reasonable sensing limits and precision, with the Clark electrode being the most commonly used. Nevertheless, its applications are constrained since its Platinum (Pt) catalyst is costly, the membrane used increases the response time, and the sensor is susceptible to biofouling.

This project explores the diamond technology attributes for a working electrode that can be included in the design of an amperometric oxygen sensor suited for harsh environmental applications. The use of boron-doped diamond (BDD) in electrochemistry is presented in [2] and [3], as a material that demonstrates a broad electrochemical potential, impressive physical and chemical durability, and long-term response stability. BDD has also proved to be environmental-friendly. These characteristics make it an ideal option for the DO electrodes. Alternatively, the properties of intrinsic diamond with graphitic-like regions are analysed to observe the electrochemical enhancements they bring. Three samples of modified-diamond with distinct manufacturing techniques are tested as working electrodes for the DO sensor. Through electrochemical experiments such as cyclic voltammetry and chronoamperometry, the electrodes are analysed and compared by sensitivity, linear response range, detection limit, and response time.

To date, few approaches have been introduced for direct dissolved oxygen measurements, including titration, fluorescence, chemiluminescence, and electrochemical sensors. Owing to its rapid response, low cost, increased sensitivity, and high precision, the electrochemical sensor gained much interest. Nevertheless, the real-time analysis of DO in industrial electrodes requires a high potential. Thus, various techniques were approached by research groups to modify the sensor and improve the correlation of reduction current on dissolved oxygen concentration.

The most common electrochemical sensors are the Clark-type galvanic ones. As explained in a 1977 publication by Schwartz, the initial Clark design has three essential elements; a Pt working electrode, an Ag / AgCl reference electrode, and an oxygen-permeable membrane [4]. During measurements, an electric potential is applied to the working electrode. This results in an oxygen reduction reaction on the surface of the electrode, which then leads to a current proportional to the oxygen level present. The electrode's reaction rate relies on the thickness of the membrane, as it takes time for the molecules to reach the cathode [5]. Thus, it can create a lag in response time. Besides, the membrane is susceptible to deterioration and fouling. Improving the durability and accuracy of sensors in extreme environments requires the design of sensors without a membrane, with durable materials that lead to high accuracy and stability in readings.

There have been reports on improved amperometric sensors without a membrane; for example, one research proposes the use of microelectrodes. Sosna et al. introduce a free-membrane oxygen sensor, designed for oceanographic purposes as well as for the data collection in water systems. The oxygen sensors record the diffusion of regulated current to a bare platinum microdisc electrode for oxygen reduction [6]. The microdisc array structure has proved to have many advantages and is also the design choice of two of the diamond electrodes in this BEng project.

In many respects, the diamond is a remarkable material, with characteristics that involve excellent hardness and module of Young, biocompatibility, optical and fluorescent characteristics, elevated thermal conductivity and electrical resistivity, chemical stability, and resistance to hostile conditions. Thus, these unique properties of diamonds make it of great interest in the study of sensors for chemical measurements. For example, Hutton, Laura, et al. reports the use of the polycrystalline boron-doped diamond (pBDD) as material for the dissolved oxygen sensor electrode. This device has a small background currents and resistance to fouling. Other advantages of the boron-doped diamond (BDD) are its resistance under extreme conditions, excellent thermal conductivity, and compatibility with both acidic and alkaline solutions [7].

Another research conducted by Ivandini, Tribidasari A., et al. proposes the study of gold-modified boron-doped diamond (BDD) electrodes for amperometric oxygen measurements but also for the identification of the biochemical oxygen demand (BOD) using a species of yeast. The gold nanoparticle altered BDD proved excellent linearity for oxygen measurements using yeast cells as a biosensing agent. The research also showed the electrodes to be highly stable [8].

Electric diamond contacts are typically made by coating the diamond with a noble metal. This method includes multiple phases, such as surface washing, development of Cr or Ti carbide, thermal rinsing, and performing a lithographic process for pixel patterning. However, metallic contacts, despite their frequent use, are not only non-ohmic but also often trigger adhesion problems, low durability, and radiation susceptibility. Thus, an oxygen sensor design that does not have metallic contacts is of great interest to this research. Wide graphitic contact on diamonds are designed and analysed in a study published by De Feudis, Mary, et al. The ohmic activity of the sample

was evaluated through various current-voltage experiments. The altered surface's characteristics showed an apparent periodicity. This finding indicated that the laser graphitisation technique is accurate and reproducible [9].

Moors, R. J., from the London Center for Nanotechnology, proposed a boron-doped diamond microelectrode. The design proves to offer an improved electrocatalytic response when compared to a BDD electrode [10]. Throughout the first term, the experiments for the BEng project were performed on this device, to get familiarised with the available laboratory equipment and experimental techniques. Moreover, the experimental cell reported by Moors, R. J. is the one utilised throughout the project, as presented in subsection 4.2.

The following chapters address the study of diamond-based electrodes. The 'Theory and Analytical Bases for the Work' chapter provides the technical knowledge necessary to carry out this research, including the theory of oxygen sensors, the principles of oxygen sensing, the properties of carbon-derived materials and the introductory theory of microelectrodes.

The 'Technical Method' chapter includes the techniques used to test experimental electrodes, with extensive information on the experimental setup, the laboratory equipment available and the configurations for all proposed electrochemical experiments.

The 'Results' chapter presents the measurements conducted with the oxygen sensor for each experimental electrode. Data is plotted in informative graphs to analyze the correlation of the sensor with the concentration of oxygen. Experimental samples are then compared to electrodes reported in various research papers. A design concept for an oxygen sensor is proposed.

The 'Conclusion' chapter summarizes all findings and their relevance to the research of oxygen sensing devices for extreme conditions. The performance of the chosen electrode with its sensor setup is highlighted, and future developments of this sensor are proposed. A design concept for an oxygen sensor is built in the Blender software and presented.

2 Aims and Objectives

The current sensor developments for DO sensing are prone to malfunction in extreme environments due to the deterioration of the material or a breakdown of the sensitivity system. The former limitation can be solved with materials of enhanced durability, while the latter indicates the production of a novel DO working electrode with improved sensitivity and accuracy. Thus, the design of a DO oxygen sensor that proves exceptional durability and accuracy in harsh environments is the primary motivation of this research.

Furthermore, in extreme conditions, sensors also require to react rapidly to monitor sudden changes in dissolved oxygen concentration in the environment. To date, few approaches for sensors have been developed for direct measurements, including titration, fluorescence, and electrochemical sensors. The electrochemical method is preferred for its rapid response, low cost, enhanced sensitivity, and high precision. Thus, the second motivation for this research is the need for a fast-responsive sensor to obtain a real-time recording of DO concentrations in the media.

This study includes the development of a novel oxygen sensor for real-time measurement of DO concentration. The new sensor tackles the issue of the possible malfunction of a dissolved oxygen sensor under harsh environmental conditions. Sensor characteristics such as sensitivity, linear response range, detection limit, and response time are evaluated and compared with results reported in other research groups.

The first objective is to familiarize oneself with all the laboratory equipment made available to the Diamond Electronics Group. This knowledge is complemented by additional research into the existing sensor technology and the various types of available working electrodes. Another essential thing to do in the early part is to learn and practice all the experimental procedures needed to analyze the performance of the electrode. These procedures include, in particular, cyclic voltammetry and step-potential voltammetry. It is, therefore, crucial to learn how to interpret output data and plot it in easily readable graphs from which analytical conclusions can be drawn.

Another objective is to evaluate the performance of three distinct modified-diamond working electrodes, primarily selected for their electrochemical characteristics and previous scientific reports. These experimental electrodes were also chosen based on the availability of the samples at the London Center of Nanotechnology, as this is a measurement-type project involving measuring samples within the scientific work of the main supervisor. Electrochemical experiments were performed repetitively, and then the results were interpreted. Characteristics like stability, sensitivity, and narrow margin are obtained via voltammetry procedures. Reconditioning of the measuring devices is needed periodically, and it represents an integral part of the reliability of the results.

The next objective is to compare the three samples, knowing the advantages and disadvantages of each. The theoretical explanation should always match the experimental findings, so attempts are made to justify one's better success in an experiment.

The last objective is to compare all three samples with those recorded by various research groups to determine their ability to function in real-life conditions. The stability of the recordings, along with the sensor's material and manufacturing process, will be contributing factors to determine if the electrodes are suitable for extreme environments.

3 Theory and Analytical Bases for the Work

3.1 Carbon Materials

Carbon is a chemical element occurring in various primary forms in nature and is the fourth most abundant substance by mass in the universe. It is a non-metallic and tetravalent element, providing four electrons that form covalent chemical bonds. Carbon atoms can bind in numerous ways, leading to very distinct carbon allotropes in terms of mechanical and electrical characteristics. Thus, an sp^1 bonding results in carbyne, the sp^2 bonding in graphite, and finally, the covalent sp^3 bonding in diamond.

3.1.1 Diamond

Diamond is a notable crystal increasingly studied in electrochemistry for its brilliant properties and is at the base of the electrodes proposed in this project. It is therefore of great interest to present and discuss its structure, properties and manufacturing methods.

3.1.1.1 Crystal Structure

Carbon presents orbital hybridization as a result of its bonding. Four hybrid sp^3 orbitals (in electron configuration) are produced by the mix of the 2s and the 3p shells in the atom. In diamond, each of those four orbitals combines with other sp^3 orbitals from four neighboring atoms and form covalent bonds, also named sigma bonds. Minimizing energy leads to the symmetrical, tetrahedral structure of four carbon-carbon bonds that are as distant as practical from one another, with a bonding angle of 109.5 degrees. Please see Figure 1 for a simplified hybridization diagram.

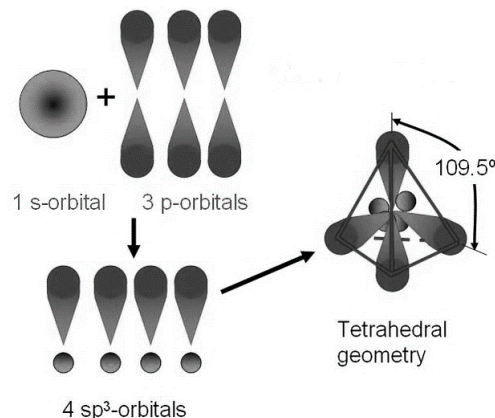


Figure 1: A Simplified Diagram for the sp^3 hybridization. [11]

3.1.1.2 Diamond Production

The natural formation of diamonds took place billions of years ago, within Earth's Crust. There, the severe heat (900 to 1,300 degrees Celsius) and pressure (45 to 60 kilobars) conditions favour the crystallisation of carbon atoms which leads to the creation of diamonds. Under these extreme environment, molten kimberlite is also produced within the Earth's mantle, expanding rapidly. This expansion allows the lava to erupt, pushing it to the surface, along with diamond carrying stones. Once it cools down, the magma solidifies to kimberlite, the primary source of natural diamonds.

The first nanoscale diamond particles were caused by detonation during the 1960s in USSR. Nowadays, there is an impressive number of procedures for the formation of synthetic diamonds. They can be produced by detonation, laser ablation, plasma chemical vapour deposition (CVD), electron irradiation of carbon onion, ultrasound cavitation and many others. Chemical vapour deposition methods can generate diamond films utilising only hydrocarbon gas in an abundance of hydrogen. This discovery has made enormous and increasing engagement of the researchers of diamond and

its application in electrochemistry. This method requires a gas-phase reaction emerging over a solid surface, causing deposition on the surface [12]. CVD film development techniques include a method of triggering gas-phase carbon-carrying precursor molecules. The reasons for using the gas phase activation are two in number and relatively straightforward. First, to establish a relatively high concentration of active carbon-containing species that break down with the development of carbon atoms once encountering a heated surface. Second, to produce a reactant. For example, hydrogen that obstructs the deposition of non-diamond carbon allotropes.

The initial diamond production using CVD had low growth-rate performance utilising low-pressure methods, which led to scepticism regarding the accuracy of this procedure. A rival technique, high-temperature / high-pressure (HPHT), became far more effective after development in the 1950s [13], and the development of low-pressure diamond stagnated. HPHT system does not replicate conditions as severe as for the formation of natural diamond. The temperature and pressure minimum to transform graphic carbon to diamond are reduced by using a metal-solvent catalyst method. Although HPHT's growth levels are outstanding, it is challenging to develop very pure diamond, since the HPHT materials sometimes contain significant quantities of nitrogen and other residues, rendering HPHT diamond unsuitable for use in electrochemistry application.

In the 1980s, S Matsumoto, from the National Institute of Inorganic Materials Research (NIRIM), developed a simple, space-constrained reactor which utilised a gas mixture of methane and hydrogen, ionised into a plasma by a heated filament, and later a microwave reactor. This latest system, named NIRIM after the institution, was far less complicated than an HPHT reactor, and it greatly enhanced diamond growth at low-pressure and rendered diamond samples far more desirable for research purposes in electronic applications [14].

3.1.1.3 Properties of Diamond

Diamond shows excellent durability and Young module, biocompatibility, optical and fluorescent characteristics, high thermal conductivity and electrical resistance, chemical stability, and resistance to hostile conditions. As mentioned, diamonds have sp₃ bondings, and the atoms form tetrahedra with four closest neighbors. The tetrahedra bonds are strong, and the diamond has the most atoms per unit volume of all materials. Hence, they are also the hardest and most shock resistant. Table 1 below presents the electrochemical properties of the intrinsic diamond, according to Wort and Balmer Wood.

Diamond has the same type of bonding and crystal structure with the semiconductors silicon and germanium. Nevertheless, the latter elements lack the high bandgap of the diamond (-5.5 eV) and its excellent insulating properties when available in an intrinsic form. This fascination with diamonds is therefore driven by both their similarity and their singularity to other elemental semiconductors. Below are enumerated the most significant characteristics of the diamond, which made it of great interest to this project:

1. Extreme Mechanical Hardness 90 GPa

Band gap	5.47 eV
Breakdown field strength	10MV cm^{-2} to 20 MVcm^{-2}
Coefficient of thermal expansion	$1\times10^{-6}\text{K}^{-1}$
Electron mobility (Hall Effect)	$4500\text{ cm}^2\text{V}^{-1}\text{s}^{-1}$
Electron mobility (Time of flight)	$600\text{ cm}^2\text{V}^{-1}\text{s}^{-1}$
Electron saturation velocity	$2\times10^7\text{ cms}^1$
Hole mobility (Hall Effect)	$1650\text{ cm}^2\text{V}^{-1}\text{s}^{-1}$
Hole mobility	$3800\text{ cm}^2\text{V}^{-1}\text{s}^{-1}$
Hole saturation velocity	$0.8\times10^7\text{ cms}^1$
Thermal conductivity	$21.9\text{ W cm}^{-1}\text{K}^{-1}$

Table 1: Properties of Diamond. [15]

2. Can withstand temperatures of 3000 °C and above
3. Highest Bulk Modulus $1.2 \times 10^{12}\text{Nm}^1$
4. Lowest Compressibility $8.3 \times 10^{13}\text{m}^2\text{N}^{-1}$
5. Highest Thermal Conductivity at room temperature $2\times10^3\text{Wm}^{-1}\text{K}^{-1}$
6. Thermal expansion coefficient comparable to that of invar (at room temperature) $0.8 \times 10^{-6}\text{K}^{-1}$
7. Broad Optical Transparency
8. Excellent electrical insulator; room temperature resistivity of 10^{16}Wcm
9. Doped diamond has a resistivity range of $10 - 10^6$; as a semiconductor with wide bandgap of 5.47 eV
10. Very resistant to chemical corrosion
11. High radiation hardness

3.1.1.4 Dopping of Diamond

Doping the diamond results in the enhancement of already existing properties or evolution of other ones, making this crystal more suitable for electrochemical application. For example, although the undoped diamond is highly electrically resistant when doped with boron (p-type doped), it becomes a semiconductor. This finding has been observed after it was reported that the deposition of materials on a diamond surface is possible through CVD. Thus, during the growth process, the dopant atoms can be inserted into the plasma-containing chamber, resulting in the formation of doped diamond films. P-type diamond with significant control over the electrical conductivity is possible through adding a dopant in the initial CVD growth process. N-type diamond is possible through introducing phosphine into the plasma. Both the n-type and p-type diamond are needed for multiple electrochemically-based studies. It is clear from Figure 2 that different activation energies are obtained by varying the insertion doses and annealing temperatures. The recognized activating energy of boron in diamonds is attained at a small doping level. In the case of higher boron doping levels obtained

by multiple implantations and annealing sequences, the activation energy is reduced. High boron concentrations in diamonds are usually preferable for electrochemical applications due to their higher conductivity [16].

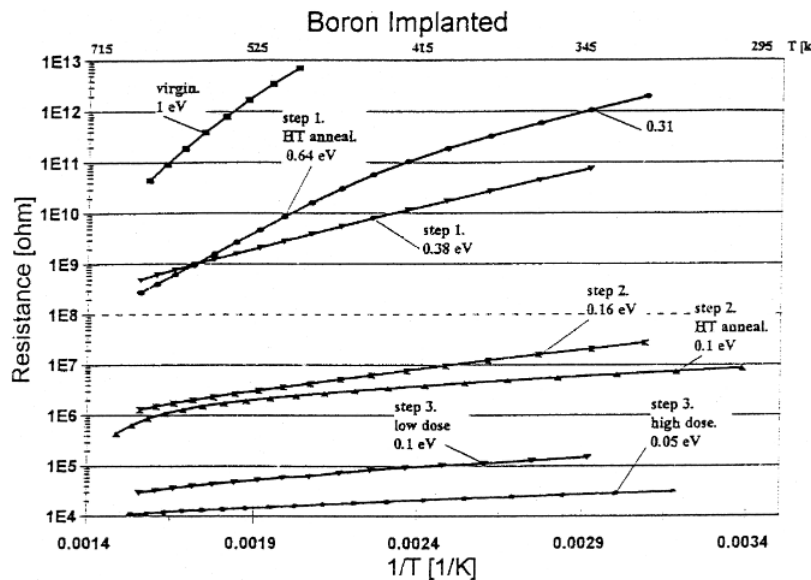


Figure 2: Resistance vs. inverse temperature for Boron implanted CVD diamond. [16]

The assumption can therefore be drawn that the boron doping level affects the electrochemical activity of BDD, such as the potential window and the conductivity. High boron concentrations in diamonds are typically better suited for electrochemical applications due to their higher conductivity. Thus, boron-doped diamond electrodes demonstrate a broad electrochemical potential in a liquid environment. This attribute allows BDD electrodes to have vast practical applications in the electrolytical determination of a range of organic molecules, such as those with large oxidation potential.

3.1.2 sp₂ Carbon

Graphite is an element formed in Earth's crust and mantle once carbon is exposed to extreme temperature (750 °C) and pressure conditions. As mentioned before, carbon is a tetravalent element with a variety of orbital hybridizations, which lead to a range of bonding structures that can create several other carbon allotropes, with distinct characteristics to the sp³ diamond. For example, graphite, an Sp₂ diamond component, is soft and conductive, while diamond is hard and insulating. The hybridisation of sp₂ leads to three sigma bonds with an angle of 120°. The remaining 2p orbital produces electrons underneath the carbon plane with simple stimulation. Such π electrons should lead to high conductivity because of the overlapping orbits in bulk materials, transparency, and poor graphite interplanar link. Graphite appears as sheets of hexagonal carbon arrays, as seen in Figure 3.

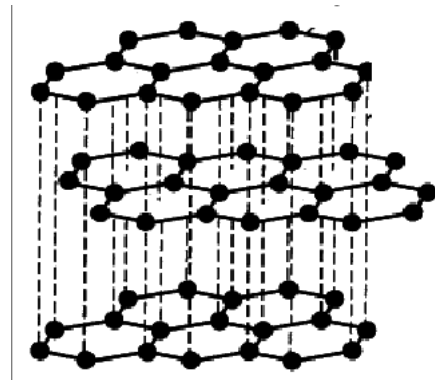


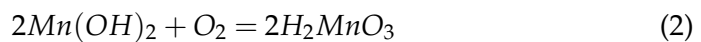
Figure 3: Structure of graphite; dashed lines represent the weak connection between the planes. [17]

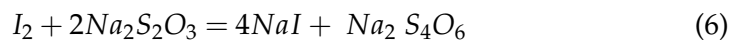
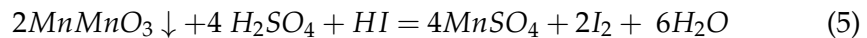
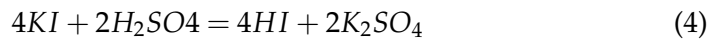
3.2 Oxygen Sensors

Oxygen sensors have a crucial role in tracking emissions for the automotive engine management, chemical process management, factory boiler control, etc. In particular, evaluating the concentration of dissolved oxygen is regarded as one of the most critical measures for the aquatic safety metrics. Fish, algae, and all other living marine organisms need the oxygen dissolved to survive. For medical applications, oxygen sensors are used for the monitoring of oxygen concentrations for respiratory gas mixtures in medical equipment, including anesthesia machines, ventilators, incubators, etc. Dissolved oxygen's measurement approaches cover the iodometric titration, the optical method and the electrochemical method.

3.2.1 Iodometric Titration

Iodometric titration is a laboratory-analytical chemical process and a widely acknowledged dissolved oxygen standard method. The iodometry method involves applying manganese sulfate and alkaline potassium iodide in the cell containing water, resulting in a solution of manganese hydroxide. The manganese hydroxide mixes with DO resulting in manganic acid. Sulfuric acid is introduced to react with the DO; potassium iodide is introduced in the reaction to separate the iodine from the rest of the solution. Starch is utilized as an index, and the iodine resulted helps to measure the DO concentration in the water sample. The chemical process of the iodometric titration is expressed below through the following chemical reactions [18]. Thus, it is clear that this is a complicated procedure, unable to be utilised for real-time continuous measurements. Moreover, the titrant can pollute the water.





3.2.2 Optical Sensing

The optical sensor centered on the concept of fluorescence quenching does not absorb oxygen and proves excellent anti-interference capability. The optical method for DO detection can be split into multiple categories, including the concept of phosphorescence quenching, the near-infrared concept, and the fluorescence quenching concept, with the latter being the most commonly applied since discovered in 1939 [19]. The sensor based on this principle determines the DO concentration by quenching the fluorescent substance following the collision with oxygen molecules. This method typically needs less frequent calibration and performs real-time continuous measurements. However, the accuracy of results is complicated to attain, and the sensor is unsuitable for extreme environments [20].

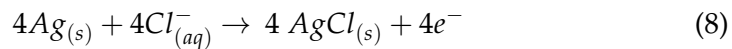
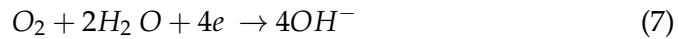
3.2.3 The Electrochemical Detection and the Amperometric Oxygen Sensor

Electrochemical detection is a commonly applied process, and it is at the base of the polarographic sensor. This approach has a reasonably high detection speed, but oxygen is consumed within the measurement process, and the sensor requires regular calibration.

The galvanic Clark-type sensors are the most common electrochemical sensors. As Schwartz explained in 1977, the original design of Clark has three main elements: a Pt working electrode, an electrode reference Ag / AgCl, and an oxygen-permeable membrane. The structure diagram of the amperometric dissolved oxygen sensor is seen below in Figure 4. Platinum and gold are often the most commonly used electrode materials because they favorise the transport-limited reduction of oxygen. Furthermore, no significant changes occur in their surface activity over time.

The membrane lets the oxygen particles to pass to the cathode and be electrolytically reduced. This reaction involves a stream of electrons at the cathode, dependent on how quickly oxygen can arrive at the electrode's surface, resulting in the electrocatalysis rate. A voltage is applied between the working and reference electrodes, and it is proportional to the electrocatalysis rate. An increase in voltage would result in an increase in the reaction

rate. However, Clark added a permselective membrane on top of the working electrode, to assure the restriction of oxygen diffusion. Over a specific voltage value, the rate of the electrocatalysis reaction will no longer increase. As such, the reaction becomes diffusion-limited and is determined by the membrane's permeability characteristics and the DO gas concentration, the metric meant to be found. The following chemical reactions describes the chemical process just mentioned:



A Clark electrode requires only two electrodes. A downside to this setup is that the reduction current always passes through the reference electrode [18]. The Ag is modified to AgCl (as seen in Reaction 8 above) when chloride oxidizes at the reference electrode, and the reaction ceases. Thus, A three-electrode setup is more favorable as the counter electrode establishes a current pathway allowing the reference electrode to stay stable on a fixed potential. Figure 4 shows the diagram of an oxygen sensor.

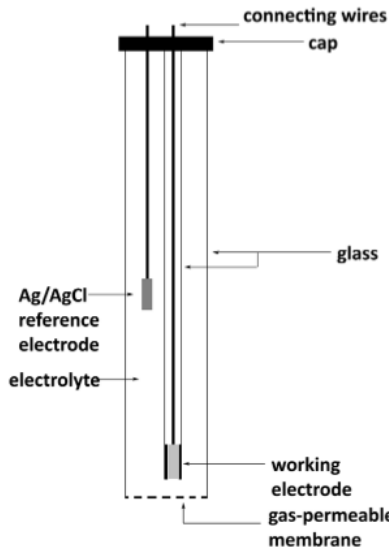


Figure 4: Diagram of the Galvanic Oxygen Sensor. [21]

3.3 Principles of oxygen sensing

3.3.1 Dissolved Oxygen

Dissolved oxygen (DO) is an indicator of the O_2 concentration dissolved in water. The presence of oxygen in water is a result of diffusion from the atmosphere, water oxidation or photosynthesis. As the number of nutrients and organic compounds from agricultural effluents, sewer waste and land erosion increase, the oxygen concentration in water could decline. The extreme

algae growth can also have a substantial effect on the DO content available. Hence, DO monitoring is especially crucial to climate scientists.

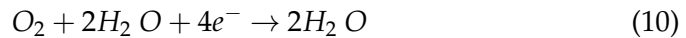
3.3.2 The Oxygen Reduction Reaction (ORR)

Oxygen calculation is centered on an oxygen-reduction reaction (ORR) at the operating electrode resulting in a measurable current. Oxygen in the proximity of the cathode is reduced to liquid-products amid the ORR. Below are Reactions 9 and 10 for alkaline and acidic solutions, respectively. The oxygen reduction reaction is an internal process of electron transfer which usually involves the use of a catalyst to achieve feasible voltages. Noble metals are usually the choice of catalysts, predominantly platinum. Experiments are usually conducted at -800 mV versus the Ag / AgCl with a potentiostat to determine the potential at the working electrode. Depending on the pH of the solution, oxygen is reduced to either hydroxide ions or water [22].

ORR for alkaline solution:



ORR for acidic solution:



Furthermore, calculation of the produced current may be connected to the sample oxygen concentration. However, as a result of this measurement method, a diffusion layer is generated from the electrode surface onto the bulk, causing oxygen depletion. This creates issues with the depletion of oxygen in tissue at the working electrode. It also affects the oxygen gradient, as discussed later. Clark-type electrodes usually benefit from a membrane that helps avoid oxygen depletion in the cell. The Clark structure contains a gas-permeable membrane, thereby preventing the diffusion of interfering particles to the electrode. Moreover, it shields the electrode from the influence of biomolecules that impede the diffusion of the analytes into the electrode layer, which would otherwise increase the reaction time.

3.3.3 Diffusion limited currents at various electrode geometries

The electrode's size is the deciding factor in the analyte's overall reaction time. As such, the larger the electrode's surface area, the higher the reacting rate with the analyte. Moreover, if the reaction with the analyte is fast enough, then the reaction rate is limited by how fast the analyte molecules reach the electrode. This is known as a diffusion rate-limited reaction. Adolph Fick described with his diffusion laws in 1995 and outlines how diffusion leads to the concentration changing over time [23]. The diffusion-reaction can be derived, by applying the appropriate boundaries, to obtain the relation between current and the area of the electrode. In electrochemistry, the Cottrell equation defines the shift in electric current over a period of time, throughout an experiment with applied potential, for example chronoamperometry [24]. Thus, the current response can be characterized by the Cottrell

equation in relation to the surface area if the applied voltage is high enough to trigger the diffusion rate-limited reaction, as written in Equation 11.

$$I = \frac{(nFA\sqrt{Dc})}{\sqrt{\pi t}} \quad (11)$$

Where I is the current in amperes (A), n represents the number of electrodes; F is Faraday's constant (C/mol); A is the surface area of the planar electrode (m^2), D is the diffusion coefficient (cm^2/s), c is the concentration in bulk solution and t stands for time.

Since the surface area and time are the only factors independent of the system, the equation can be seen as inversely proportional to the time period. As a result, the current is expected to begin with a high value and decrease with the increase in time. The diffusion field is weak the moment the voltage is applied, over time the scope of the electrode expands in the cell, causing the diffusion field to increase. The concentration gradient is reduced, and the reaction rate and current decrease accordingly.

Equation 11 for the planar case described above does not extend to the disc microelectrode. With the increase of circumference to area ratio, the edge effect becomes considerable, meaning the diffusion component at the edge of the disc is more significant in comparison to the one present the planar electrode. Recent reports [25] show that in a small constraint of time, the thickness of the diffusion layer is not greater than the electrode's radius and the current adheres to the Cottrell equation. However, over time, the diffusion field becomes more extensive than the electrode's radius, and the edge effects dominate. The equation for the microelectrode's steady state current is shown in Equation 12. Because the equation is missing the component (present in the equation for the planar electrode), at a larger time value the current is expect to deviate higher than the Cottrell plot.

$$i = 4nFDCr \quad (12)$$

3.3.3.1 Cottrell Plot

When the reduction reaction is constrained by the diffusion rate at the working electrode and the configuration of the electrode is well established the Cottrell equation should be used to describe the original current. It may be possible to have an extra current component, the capacitive double-layer current. The steady-state current, or reduction current will be proportional to the oxygen levels. After a while, it ought to be seen that the reduction current is greater than it was estimated by the Cottrell formula. It should be mentioned that the double layer current can be estimated by the following formula:

$$I_{capacitive} = Electrode\ Area \times C_{dl} \times scan\ rate \quad (13)$$

Where C_{dl} is the double layer capacitance, specific to the electrode surface.

3.3.4 Microelectrodes

Microelectrodes have been increasingly used for amperometric gas sensors in recent years. They offer high sensitivity, rapid response time, minimised

costs, low detection limit, and easily reproducible geometries. In the 1980s, the invention of microsensors became a breakthrough in electrochemistry. The microelectrodes and their electrochemical properties are presented in this section as discussed in references [26], [27], [28] and [29]. With a microelectrode, the reduction current can quickly develop at the working electrode as it functions at an optimum voltage (rarely passes 1.5 V in aqueous media) to reach a diffusion-limiting reaction rate [26]. The resultant region of diffusion is limited and not as prone to diffusion that increases currents and fluctuations. Moreover, it would make it insensitive to the kinetics of reduction reactions, allowing it to operate across a broad pH spectrum. The steady-state current is also predominantly unaffected by the voltage applied, which means that the variations in reference voltage become less relevant to the measurements.

3.3.4.1 Mass Transport

Fick's second law defines the diffusion of electroactive product across spherical electrodes. Fick's law has been previously mentioned in Chapters 3.3.3 and 3.3.3.1, but in this section is discussed in more detail. Via a Laplace transform approach, the current density can be written as in Equation 14:

$$I_d = \frac{nFDc}{r_s} + \frac{(nFA\sqrt{Dc})}{\sqrt{\pi t}} \quad (14)$$

The second element of Equation 14 is the transient element and is often prevalent when considering an electrode of 0.1 cm radius. However, this is not the same for a microsphere, where both the transient and the steady-state components are important. Thus, for a microelectrode, three forms of diffusion can be identified at different times throughout the experiment [26].

1. Short times

When considering short periods of time, the second term from Equation 14 is considerably bigger than the first; thus, the current density is determined by Cottrell. A transient would then be found in the same form as for the planar electrode. The equation may be written as:

$$I_d = \frac{(nFA\sqrt{Dc})}{\sqrt{\pi t}} \quad (15)$$

2. Longer times

After a longer period of time, the transient current density reduces to a marginal amount, the current density attains a steady state value equal to the first term from Equation 14. The steady-state current density is inversely proportional to the radius. This property is useful in the study of the electrode's kinetics.

$$I_d = \frac{nFDc}{r_s}; \quad (16)$$

3. Intermediate Times

For intermediate times the diffusion regime and both elements of Equation 14 must be considered. Generally, the microsphere formulas can be

altered to conform to the microdisc by approximation $r = \pi a/4$; a represents the disc radius.

$$I_d = \frac{4nFDc}{\pi a} + \frac{(nF\sqrt{Dc})}{\sqrt{\pi t}} \quad (17)$$

Thus at short and long times the diffusion at microdisc can be represented by the following: For steady state current density:

$$I_d = \frac{4nFDc}{\pi a} \quad (18)$$

Thus the current will be obtained by multiplying Equation 18 by πa^2 :

$$I = 4naFDc \quad (19)$$

3.3.4.2 Discrimination Against Charging Currents

When a working electrode is inserted in a cell containing electrolyte, a typical surface charge arises. Therefore, if an electrode's voltage is modified, a charging current will travel as electrons pass towards or outwards from the electrode's surface. This current supplements the Faradaic reaction and interferes with the measured data [29]. The charging current can be expressed as:

$$I_d = \frac{E_2 - E_1}{R} \exp\left(\frac{-t}{RC}\right) \quad (20)$$

When the capacitance is proportional to the area, the term RC reduces as the microelectrode is shrunk. As a result, the charging current I_c is smaller. The response time is quicker and the charging current is less significant. A nearly identical principle extends to other geometries.

The reduction of the charging current may be favourable in a variety of experiments. For potential step voltammetry, for example, the experimental response is not interfered by charging currents, and the linear flux of electroactive species is stronger. Thus, the electrode will benefit from a lower detection limit. Moreover, for cyclic voltammetry experiments, higher scan rate values may be applied.

Within linear diffusion situations, the aforementioned I_d (See Equation 20) is relative to the square root of the scan rate, whereas the charging current increases with the increase in scan rate. Thus the charging current is increasingly significant at higher scan rates and will gradually interfere with the output data. Yet such distortions arise for a microelectrode only when the scan rates are greatly larger.

3.3.4.3 Reduced Distortion from IR Drop

The current flow in a solution involves a potential resulting in the drop of a fragment of the potential from the working and reference electrodes. Therefore, it is important to reduce the interference of the uncorrected iR, from the experimental response. Otherwise, that interference would make the response unfit for interpretation. One method to eliminate this distortion for large electrodes is to use a three-electrode setup, instead of two. However, the microelectrode offers another method. Since iR is proportional to the radius, for a non-steady state, the iR drop becomes less significant with the reduced size of the microelectrode.

3.3.4.4 Reduced Area

Many microelectrode implementations are essentially attributed to their reduced scale. Hence they permit measurements at small sample sizes and have been increasingly used in amperometric sensors.

3.4 Defining the extreme environment conditions in the context of the project

Typically, extreme environmental conditions are defined by intense motion, radiation, electromagnetic disturbance, high-pressure, and high-temperature states. Since this project was proposed as a result of the industrial collaboration between Diamond Electronics Group with BAE Systems Maritime Ltd., the extreme conditions are considered to be those a submarine must withstand. Thus, this project is explicitly focussing on high-temperature and high-pressure situations, plus the added stressors of seawater corrosion, and various forms of shock. At 300 m underwater the submarine is withstanding 3,000 kPa of water pressure. Moreover, the equipment is typically designed to tolerate temperature cycling within a range from -2°C to $+32^{\circ}\text{C}$, and 3,5 per cent salinity [30]. Oxygen sensors are also exposed to water shocks, and thus for its design, sturdy steel materials are to be considered, however iron should be avoided. Diamonds are the ideal choice for electrode material due to their excellent durability and the ability to withstand temperatures of more than 3000°C and pressures of 600 GPa (please refer to section 3.1.1.3).

4 Technical Method

4.1 Electrochemical Measurements

Three electrodes are added in the cell containing the solution to be analysed. The experiments in this research mostly have deionised (DI) water as the experimental solution. The current-potential curve is evaluated by recording the current output when a potential is applied with a potentiostat; this is the procedure used in the research. Alternatively, the outputted potential could have been recorded as the current is passed through a galvanostat. A Metrohm Autolab "PGSTAT20" is a compact modular potentiostat/galvanostat used throughout this project. All experiments are carried out at room temperature, of circa 25, with no significant changes over time.

The three-electrode setup includes an Ag/AgCl reference electrode, a Pt foil counter electrode and a working electrode. The three samples of diamond electrodes will be used as working electrodes, in turns. The control software that recorded all measurements was the Metrohm NOVA 2.1. The data recorded by the experimental sensor was checked for accuracy with a Pyroscience 'FirestingGO2' optical oxygen probe, the functional principles of optical probes can be found in Chapter 3.2.2. On MATLAB the data from NOVA 2.1 and FirestingGO2 were concatenated, and all experimental data was plotted into graphs. In section 5, a design concept for the oxygen sensor is built in Blender graphics software.

4.1.1 Cyclic Voltammetry

Cyclic voltammetry is an efficient electrochemical method used to analyse the reduction and oxidation processes of the sample. The potential varies between positive and negative peaks at a steady rate. The current is measured and plotted as a function of the given potential applied to the working electrode, while a reference electrode maintains a constant potential [31]. This technique is important to our study for several reasons, one of which is that it helps investigate the type of reaction underway, if it is a reversible reaction or not. Besides, this technique helps to determine whether reactions are affected by mass transport or kinetic limitations. Furthermore, since oxygen is proportional to the current, oxygen levels can be determined by plotting the current over the calibration curve.

The forward scan is from point a to d, and the reverse scan is from d to g. Point d is considered the switching potential. By the time it reaches the d value, the potential would have been large enough for the analyte to undergo oxidation or reduction. In the forward scan the potential scans positively, and the analyte undergoes reduction; in the reverse scan, the potential scans negatively and the analyte undergoes oxidation (as seen in Figure 5). However, there are analytes at which first occurs oxidation, followed by reduction, for which the potential scans would be reversed. Another important thing to mention is that the slope of the plot gives the scan rate.

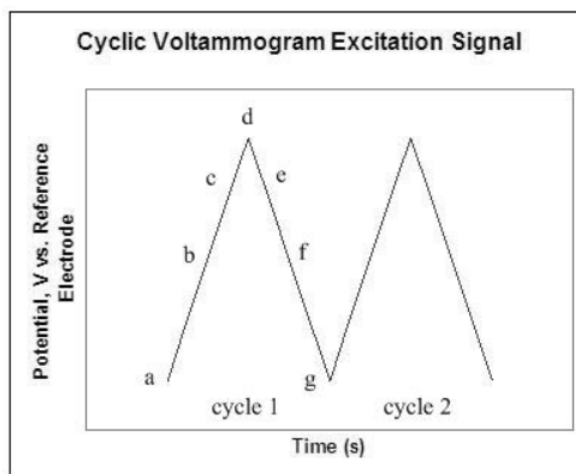


Figure 1: CV Excitation Signal

Figure 5: CV Excitation Signal [32]

Plotting the data for the output current vs the potential gives the cyclic voltammogram as seen in Figure 6. The reduction process is from the initial potential at a to the switching potential at d, where the cathodic potential (E_{pc}) is attained when the entire substrate of the working electrode has been reduced. Then, the potential is scanned positively from the point d to g, and the anodic peak potential (E_{pa}) is reached when the electrode has been entirely oxidised. Moreover, the labeled I_{pc} and I_{pa} represent the cathodic and anodic currents, respectively.

The cyclic voltammetry procedures are run through Nova 2.1, at an upper

potential of 1 V and a lower potential of -1. The same process is performed at different scan rates from 0.05 V/s to 4 V/s, to observe any changes in current. It is also important to mention that the voltammetry procedure from Nova, first scans positively (from smaller potential to higher potential), and then negatively (from peak potential to low potential). Thus, in the first scan the analyte will first go through oxidation, followed by reduction in the second scan.

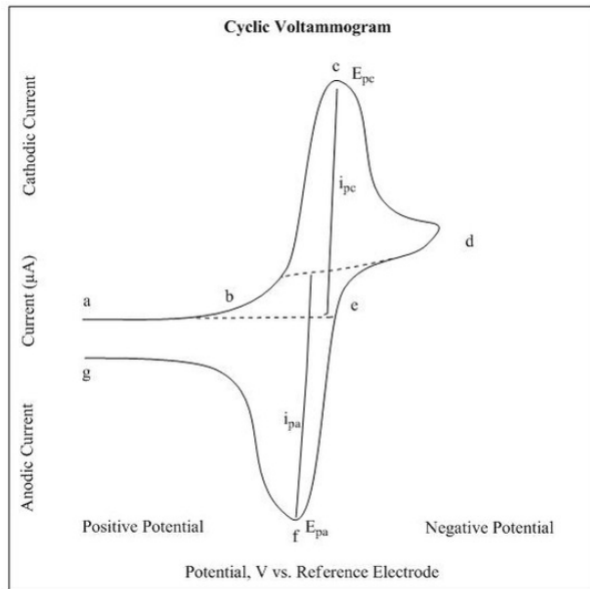


Figure 6: Cyclic Voltammogram [32]

4.1.2 Potential Step Voltammetry

For the potential step voltammetry, the voltage applied to the electrode is immediately jumped from one value to the other (Figure 7), and the resulting current is recorded and plotted against time. This experimental technique is helpful for the research of specific electrochemical events that may be activated or inhibited at particular potentials.

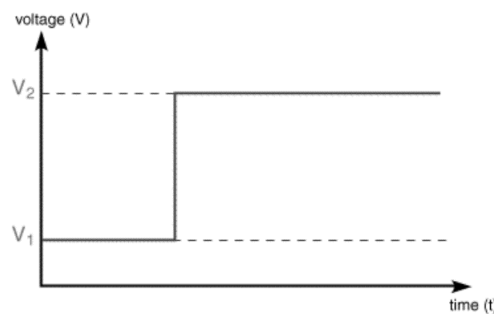


Figure 7: Potential Step [32]

In this research, step voltammetry is mostly used to conduct experimental procedures in current regions that present diffusion and mass transfer

limitations. The current automatically rises after the voltage shift and then decreases in the proportion of time. While the electrolysis proceeds, the substance will diffuse away from the electrode more, resulting in a decrease of the concentration gradient, with the concentration gradient decreasing the reactant availability to the surface, thereby reducing the current.

The measurement process is accompanied by the cleaning pulse cycle. Repetitive measurement pulses can be carried out with good reproducibility when followed by a short electrochemical cleaning period [33]. Thus, from Nova 2.1, we set a measurement pulse of -0.8 V that runs for 50 seconds, followed by a cleaning pulse at 0.2 for 3 seconds, as seen in Figure 8.

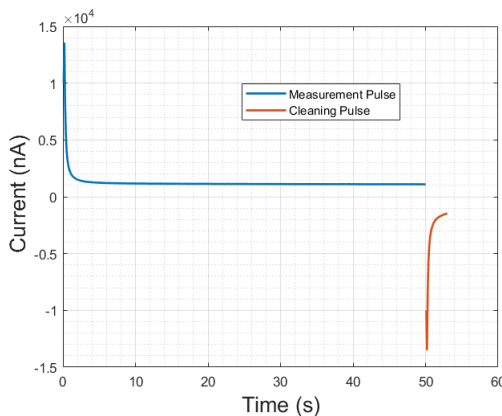


Figure 8: The Measurement and Cleaning Pulses

Controlled injections of a balanced gas mixture of Oxygen and Nitrogen determine the amount of dissolved gas in the deionized water cell. The system involves two mass flow controls with a multi-channel readout. A combination of nitrogen and oxygen has been pumped through the gas dispersal tube into the cell. The levels of oxygen are recorded by the FireStingGO2 optical oxygen sensor. The oxygen concentration can be adjusted in the cell by calibrating the Mass Flow Controller while checking the readings of the optical sensor.

4.1.3 Performance Indices of Oxygen Sensors

Amperometric oxygen sensors have an increasingly pivotal role in pollution control, medical systems, industrial and automotive industries. The basic performance parameters of the sensor system are discussed here.

4.1.3.1 Stability over time and Current Drift

Stability over time is a precision metric determined under continuous measurements at fixed oxygen concentration and unchanged operating procedures. The drift in current is the difference between the reduction currents of the initial and final measurements, and it is used to analyse the sensor's stability. Another definition of drift is as a prolonged and sometimes gradual output alteration over time caused by changes in the sensor's metrological characteristics [34]. The causes of drift are varying reference potential due to the contamination or degradation of the reference and counter electrodes,

modification of electrolyte concentration or solution's pH, contamination of the experimental electrode. Another cause of drift is the change of the diffusion layer that restricts mass transfer. Alterations of the working electrode cannot influence the sensor unless the mass transfer will no longer be at the rate-determining step. If the sensor operates in a mixed kinetic form, the parameters could change, and the reading will no longer be accurate [22]. Stability over time is evaluated by calculating the drift in current output from prolonged oxygen measurements at fixed O_2 levels.

4.1.3.2 Response time

Response time is among the key indices of accuracy for sensors. This metric defines the amperometric sensor's dynamic attributes given changes in measurement. The sensor reaction time or T_{90} is considered the time for the current to hit 90 per cent of the reduction current, given that this value correlates to the analyte's concentration in the solution [35].

4.1.3.3 Linearity

Because the transfer of electrons is faster than the mass transfer rate of oxygen, the current is determined by diffusion, not the kinetics of the electrode's reaction [36]. As a result, the current increases linearly for a wide spectrum of concentrations. The linearity corresponds to the DO concentration levels for which the output reduction current is proportional to that concentration. The sensor's linearity is expressed as the range between the lowest and the maximum oxygen concentration that is estimated with presumed accuracy. For this project's results, the linearity is evaluated through continuous steady-state current measurements at increasing oxygen concentrations.

4.1.3.4 Sensitivity

The sensor's sensitivity is affected by the area where the oxidation-reduction reaction happens. The active surface area is defined as the region between the analyte, the electrode and the electrolyte since only there the reaction takes place [37]. Nanostructures are capable of significantly increasing the active surface area and improve the sensitivity of the electrode [38]. The indicative of sensitivity is the slope of the calibration curve for output signal over O_2 concentration, and its expressed as nAL/mg.

4.1.3.5 Accuracy Detection Limit

The accuracy of the results of the sensors is analysed through means of a calibration curve of output signal over O_2 concentration. The value of R^2 gives the coefficient of determination (correlation) and is calculated in MATLAB. The detection limit is given by the lowest oxygen concentration that is estimated with presumed accuracy by the sensor's output.

4.2 The Design of the Electrochemical Cell

The optical sensor and the experimental electrode are set in proximity of one another on the coupling plate, to avoid a lag between the responses of the

working electrode and the optical oxygen sensor, at variations of the oxygen gradient. The coupled sheet is designed in such a way to expose the electrodes to the DI water on the top and make the electrical contact on the back. The liquid is held in a glassware, refitted to be used as a flat electrochemical cell. Viton circular rings are used to seal the cell and the electrodes to some polypropylene sheets. In order to create a permanent sensor frame, threaded stainless steel rods were used. The reference electrode, the counter electrode, along with the glass/ceramic sparger, were placed in the cell. Figure 9 represents the experimental setup, as designed by R.J. Moors for similar experiments for the Diamond Electronics Ltd [10].

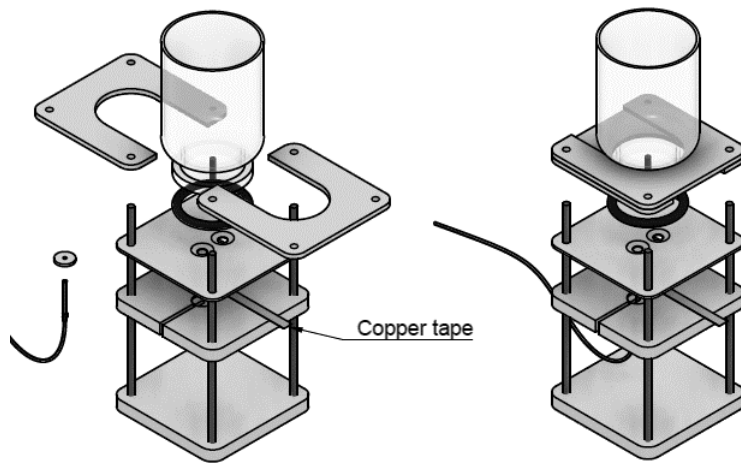


Figure 9: The Experimental Setup for the DO Sensor [10]

4.3 The fabrication methods of the working electrodes

As previously mentioned, the setup of the sensor comprises three different electrodes; the working, reference, and counter electrodes. The diamond samples will occupy the role of working electrodes, in turns. Their suitability as electrodes determines the performance of the oxygen sensor. As such, their fabrication methods shall be discussed next. These electrodes were also chosen based on the availability of the samples, as this a measurement-type project involving measuring samples within the scientific work of the main supervisor. The three samples were built, modified, and are property of Diamond Electronics Ltd.

4.3.1 The Pt-on-diamond microelectrode array

For this fabrication process, the diamond of choice was a Boron-Doped Diamond (BDD). The BDD was then coated with a 4nm Pt film. The electrode and Pt film were annealed to allow the nano-particles to develop on the electrode's surface. The microelectrodes were created by passivation with an SU-8 layer which left a microelectrode array exposed. The designed holes form channels down to the conducting substructure of the electrode. SU-8

is a photo-resist that will be utilized as a permanent mask for obtaining a microelectrode array on conductive BDD electrodes. This photo-resist is the perfect choice in this case because of the need for robust characteristics and a broad aspect ratio geometry with excellent chemical compatibility, and it is also preferred for economic and straightforward sensors. Figure 10 shows the magnified image of the Pt-on-diamond microelectrode array.

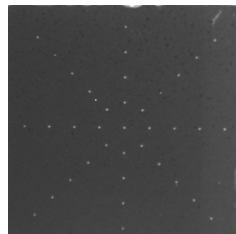


Figure 10: Pt-on-diamond microelectrode array [10]

4.3.2 The 3nm-Pt-on-BDD electrode

The next electrode to be analysed is an electrode of 3nm platinum nanoparticles on diamond. Nanoparticles have been formed through a gas phase synthesis process. In particular, the nanoparticles are developed using a gas-phase magnetron-sputter condensation. The rapid kinetics and non-equilibrium processes involved enable the controlled production of versatile Pt NPs. The synthesis of the Pt NPs can be broken down in four steps, aggregation, coating, mass sorting and deposition. Gas-phase synthesis is suitable for oxygen sensor devices since the catalytic activity is determined by the size of NPs, which this process offers great control over. Moreover, it offers high chemical purity because organic solvents are avoided. As a result, the gas-phase synthesis method used for the deposition of Pt NPs on the BDD electrode exhibits great potential for the development of an oxygen sensor with increased efficiency.

4.3.3 The Graphitic Microelectrode Array

Microelectrodes have multiple advantages which are discussed in this project and reported in multiple research papers. However, the drawback the Pt-on BDD microelectrode array has is that it contains a passivation layer, which is usually susceptible to considerable damage. Thus, the scope of fabricating a Graphitic Microchannel Array electrode is to keep the advantages the microelectrodes offer, without the drawback the passivation layer adds. This scope is reached by laser graphitising the microdisc conductive features directly on the electrode. A cylindrical piece of intrinsic diamond was treated by laser, with the surface presenting graphitic material as a product of the cutting. Numerous individual microelectrode structures are made on the surface of the intrinsic diamond to facilitate electrochemical analysis. The process of laser graphitisation generates conductive microchannels directly on the diamond, without the need for passivation. The microelectrodes from the diamond's substrate form one large electrode. Electrical connections are produced through lasering from the top to the bottom of the electrode. The

intrinsic diamond is kept intact and may be used as to seal the window for sensor systems working in extreme environments.

This process ensured that the sample would benefit from high-purity substrates without involving growth stages or complex lithographic processes. The sp₂ regions are promoting increased electrocatalytic oxygen reduction. Most important of all, it benefits from the advantages of a microelectrode array without using a passivation layer.

5 Results

5.1 Pt-on-diamond microelectrode array (PtDMA)

The first experiment consists of running a chronoamperometry procedure from NOVA 2.1 for continuous loops at increasing oxygen concentrations. The procedure begins with an oxygen concentration of -0.36mg/L. It reaches 35mg/L within 1 hour and 25 minutes. The Nova procedure stopped after 88 loops, when the DI water reached saturation. This number of repetitions resulted in 88 data sets for the measurement pulses. Figure 11 shows the data for stabilized reduction current and the data for oxygen concentration, plotted over time. The reduction current is increasing with the increase of O₂ concentration in the cell.

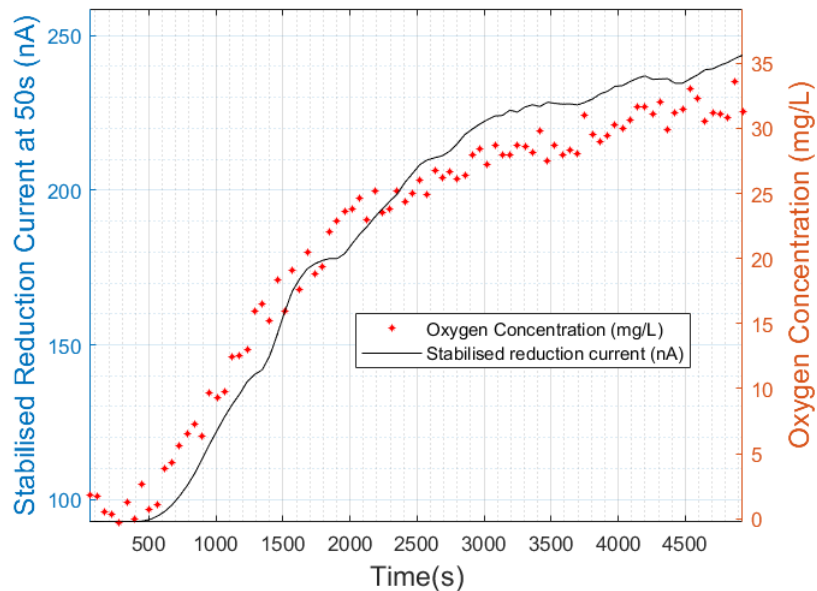


Figure 11: Data for stabilized reduction current and for oxygen concentration, plotted over time for the Pt-on-diamond microelectrode array

The plot of the sensor's reading vs parameter value indicates the calibration curve of that sensor. Thus, as seen in Figure 12, the data for the reduction current plotted against the data from the optical oxygen sensor shows the calibration curve. To better observe the relationship between reduction current and oxygen concentration, the data from the working electrode was plotted

against the readings of the optical oxygen sensor. The gradient and intercept were calculated using MATLAB.

The equation for the plot is as seen in Equation 21:

$$\text{Reduction Current} = (3.479 \times \text{Oxygen Concentration}) + 106.678 \pm 1.439 \quad (21)$$

The gradient and intercept are given by:

$$\text{gradient} = 3.479 \pm 0.057 \quad (22)$$

$$\text{intercept} = 106.678 \pm 1.439 \quad (23)$$

Knowing the intercept and gradient values and modifying the calibration curve to compute the signal conversion calculation, the following Equation 24 results:

$$\text{Oxygen concentration (mg/L)} = \frac{\text{reduction current} - 106.678 \pm 1.439}{3.479 \pm 0.057} \quad (24)$$

Using MATLAB, the graph of stabilised current against oxygen concentration has the following characteristics:

- The coefficient of determination (correlation) is: $R^2=0.977$
- The root mean squared error is: root mean squared error=6.66

As it can be observed in Figure 12, the fit is fairly linear and the coefficient of determination R^2 is equal to 0.977. The intercept from 23 can be interpreted as a background current. Its presence causes a rise in the error value at oxygen concentrations lower than 3-4mg/l, where there is a significant divergence from linearity. Moreover, the precision of the sensor readings seems to be heavily reliant on the oxygen levels. Errors become steadily smaller than 3% for oxygen levels higher than 20mg/L. The graph also shows error fluctuations between 10-15mg/L and 20-25mg/L, that may be due to a greater oxygen flow between those periods, which resulted in a less reliable steady current. The sensitivity of the electrode is of 3.479 ± 0.057 nA per mg/l of dissolved oxygen. Response time was found to be of 4.9 s at 3mg/l O_2 concentration level, given a steady state current of 120 nA.

For 50 minutes, periodic potential step cycles were performed and the measurement pulses recorded at constant O_2 concentration. This experiment shows the stability of reduction current with time. The reduction current had a drift of circa 25.62% between the first 10 cycles and the last 10 cycles. This current increase may indicate a change with solution's pH over time. When the reaction rate is partly kinetically constrained, pH variations in the liquid may influence the reaction speed. The length of the cyclic voltammetry procedure could have resulted in unwanted CO_2 entering the water in the cell leading to the forming of $H_2CO_{3(aq)}$, that can disassociate and reduce the protons' pH value.

To evaluate the reasons for the poor stability of the sensor, Chapters 3.3.3, 3.3.3.1 and 3.3.4 should be regarded informatively. If the applied voltage triggers the diffusion rate-limited reaction, then the current response can be characterised by the Cottrell equation. However, over time, the diffusion field becomes more significant than the electrode's radius, and the edge effects

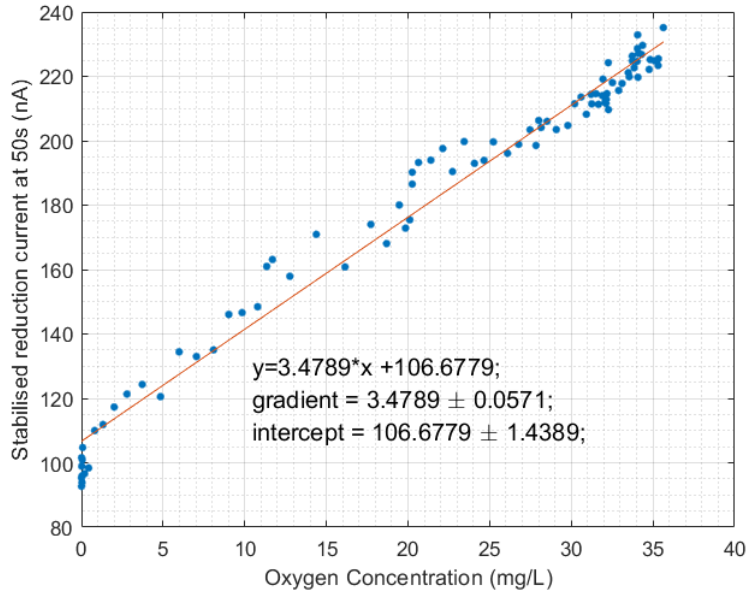


Figure 12: Calibration Curve for Stabilised Reduction Current at Increasing O₂ Concentrations for the Pt-on-diamond microelectrode array

dominate. Thus, with time, the current is expected to deviate higher than the Cottrell plot. This behaviour is seen in Figure 13 with the steady-state current plotted against $\frac{1}{\sqrt{time}}$, for a constant oxygen concentration of 11mg/l. The initial measurement period (right side of the figure) shows a deviation from the Cottrell equation. However, when $\frac{1}{\sqrt{time}}$ is between 0.4 and 3, the current respects the Cottrell plot and fits the track reasonably. In the Cottrell plot shown in Figure 13, the current deviates higher than predicted by the Cottrell formula. This is due to significant “edge effect” contribution, at high time values. The Cottrell line fitting is given by: $y = 151.52 * \frac{1}{\sqrt{time}} + 77.424$. At a large time, value ($\frac{1}{\sqrt{time}} = 0.3$; 11s from when the cycle starts), the current remains at a steady value of approximately 140 nA. This is an indicative that after a period of time, the current is starting to reach stability, due to the steady-state current of the microelectrode. This response time is higher than that reported in a research paper [39] which sustains that the current of the microelectrode should achieve steady state within 5s of starting the measurement. Thus, the steady value of 140 nA could also be explained by the capacitive effect or by the presence of a high diffusion field, a result of heat transfer and stirring in the cell.

A cyclic voltammetry was conducted for the usual experimental electrode configuration with increasing scan rates of 0.05 V/s, 0.5 V/s, 1 V/s and 1.5 V/s, as seen in Figure 14. It demonstrates that an increasing scan rate corresponds with an increasing current. It is clear that higher scan rates result not only in increasing peak currents, but also in shifts of the potential to increased positive values. At the current peak is where the voltage forces the increase of reaction rate to cause complete species depletion. Thus, from here there is a decline in current as the diffusion field expands, the transport rates reduce, and the current becomes the Cottrell current. The reduction peak

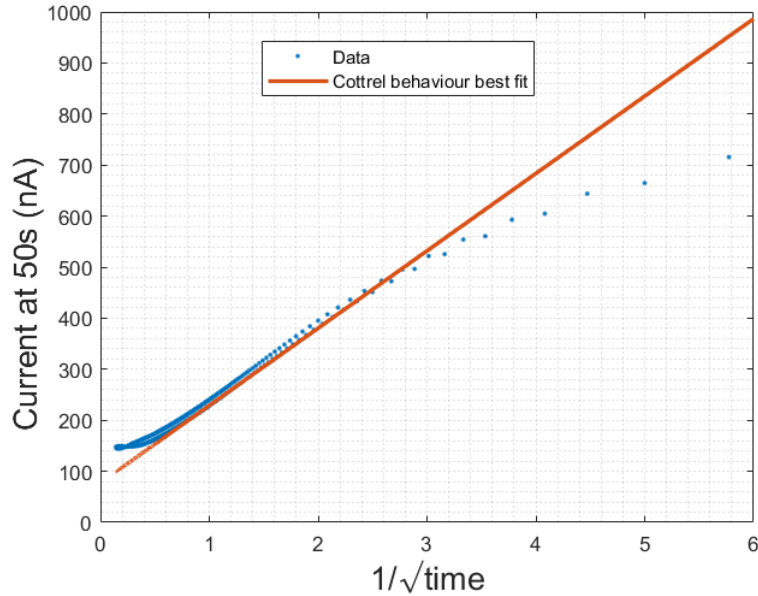


Figure 13: Cottrell plot and Reduction current vs $\frac{1}{\sqrt{\text{time}}}$ for 11mg/l O₂ concentration for the Pt-on-diamond microelectrode array

current increases with the increase of scan rate. With the output current values being proportional to the square root of the scan rate, it is clear that the reduction of DO at the surface of the experimental probe is determined by diffusion. The increase of current peak with increase in scan rate may also be explained by the highly active material concentration of the surface of the Pt-on-diamond microelectrode array.

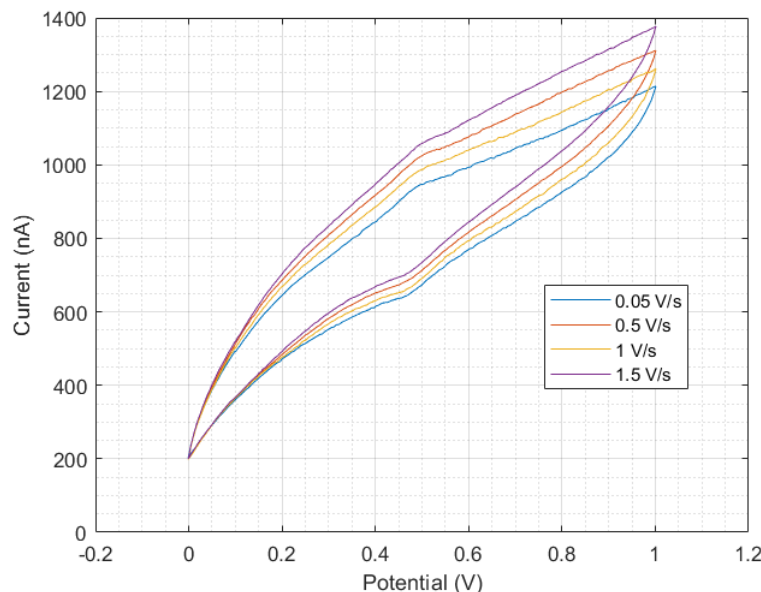


Figure 14: Cyclic Voltammetry at increasing scan rates of 0.05 V/s, 0.5 V/s, 1 V/s, 1.5 V/s for the Pt-on-diamond microelectrode array

Figure 15 shows the loops at scan rates of 4 V/s, 7 V/s and 10 V/s at increasing current, plotted against applied potential. Once again, the current value is shown to be proportional to the scan rate, as the current increases with the increase of the scan rate. Sp2 carbon within the experimental sample is capable of catalyzing an ORR while boron diamond cannot. The cathodic peak current where ORR happens for the 4V/s voltammogram is shown in the graph, and has a value of 2588 nA. Comparing Figure 14 and Figure 15, it can be seen that increasing the scan rate restores the reversibility of the voltammogram. The separation between the anodic and cathodic peak increases.

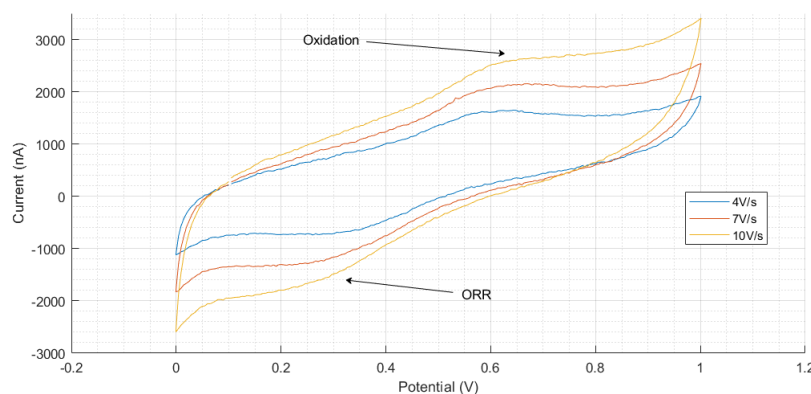


Figure 15: Cyclic Voltammetry at increasing scan rates of 4 V/s, 7 V/s, 10 V/s for the Pt-on-diamond microelectrode array

5.2 3nm Pt NPs on BDD electrode (PtBDD)

The second sample being studied is a 3nm Pt nanoparticles (NPs) on BDD electrode. NPs have been formed through a gas phase synthesis process. This technique offers the sample great catalytic activity and chemical purity. Moreover, it does not present a passivation layer, thus it is less susceptible to deterioration and scarring.

One of the most significant features of the amperometric oxygen sensor is its stability over time. Figure 16 shows the first 4 measurement pulses for the stability test. It also indicates the starting reduction currents is of 1218 nA, which is almost 13 times larger than the starting current for the microelectrode disc. This current increase is due to an increase in the surface area.

Figure 17 represents the last 4 measurement pulses, after 50 minutes. The current is at 868 nA, suggesting the stabilised reduction current decreased by 1.4%. It demonstrates better long-term stability than the Pt-on-diamond-disc microelectrode, which had a drift in current of circa 25.62% over the same period of time.

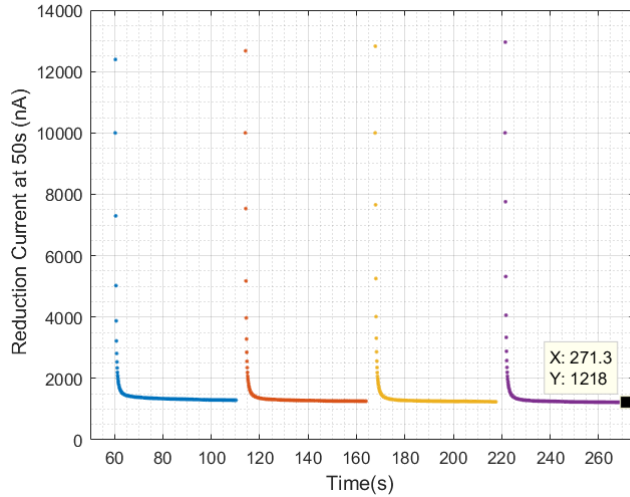


Figure 16: First four measurement pulses for the stability test for the 3nm NPs Pt on BDD

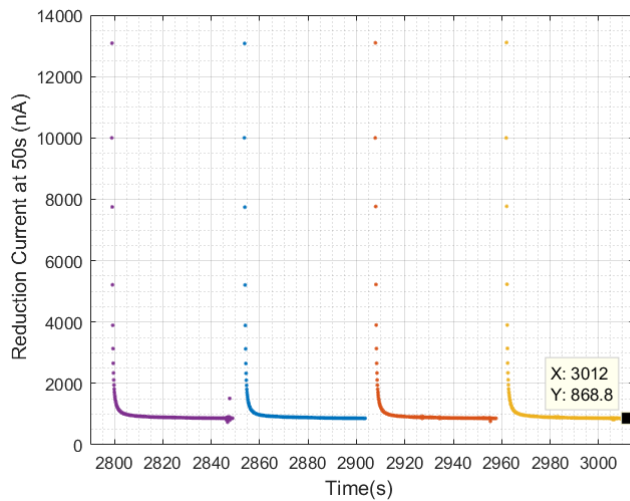


Figure 17: Last four measurement pulses for the stability test for the 3nm NPs Pt on BDD

Figure 18 represents the Cottrell plot in which the output current is shown over the inverse square root of time, for the experimental electrode at 10 mg/l oxygen concentration. Since the PtBDD is a planar electrode, the Cottrell plot appears linear in the direction of its origin. This result proves the two processes the O_2 goes through once it spreads through in the cell. First, it dissolves into the aqueous solution and then it scatters onto the sample. The plot appears to deviate only slightly from the Cottrell plot after an extensive period, equivalent to the left side of the figure. This deviation is because, in a macro electrode, the diffusion field is so large at high t that it is considerably disturbed by convection and other fluid currents which cause disturbances that intensify diffusion. Hence the Cottrell situation no longer defines it well as it specifies diffusion-limited.

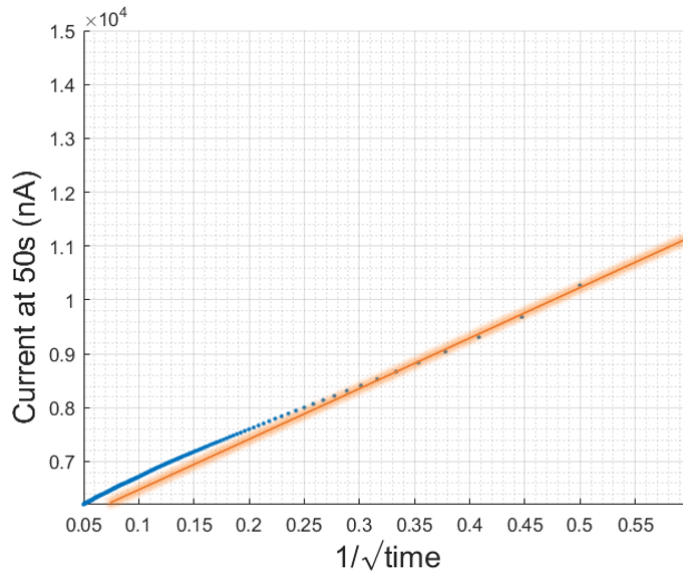


Figure 18: Cottrell plot for the PtBDD electrode

Figure 19 shows the voltammogram for the PtBDD electrode at 7mg/l O₂ concentration for different scan rates of 2.5V/s, 3V/s, 3.5V/s, 4V/s, and 4.5 V/s. Relative to the increasing scan rates, the reaction has rapid reaction kinetics, this results in the increase in current peak at the same potential. With the output current values proportional to the square root of the scan rate, it is clear the ORR on the surface of the experimental probe is limited by diffusion. The increase in current peak with an increase in the scan rate is also caused by the great concentration of active material at the surface of the PtBDD electrode.

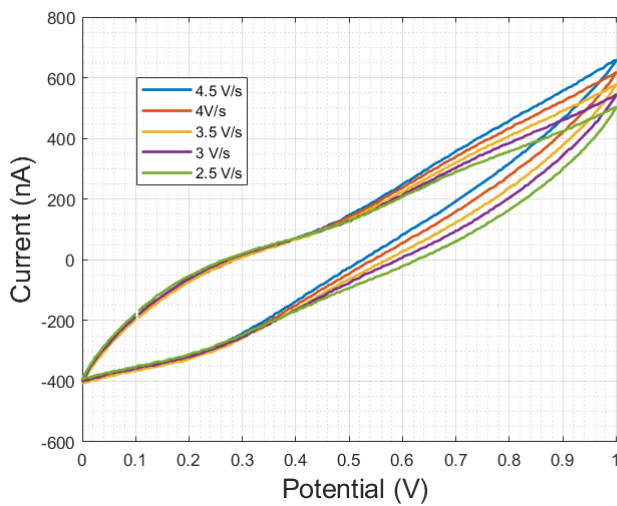


Figure 19: Cyclic Voltammetry at increasing scan rates for the Pt-on-BDD electrode

Figure 20 shows the Cyclic Voltammetry at higher O₂ levels. When doubling the O₂ concentration to 14mg/l, a sp2 oxidation peak is found on the

reverse scan, at a voltage of 0.3V, while no obvious reduction peak could be observed.

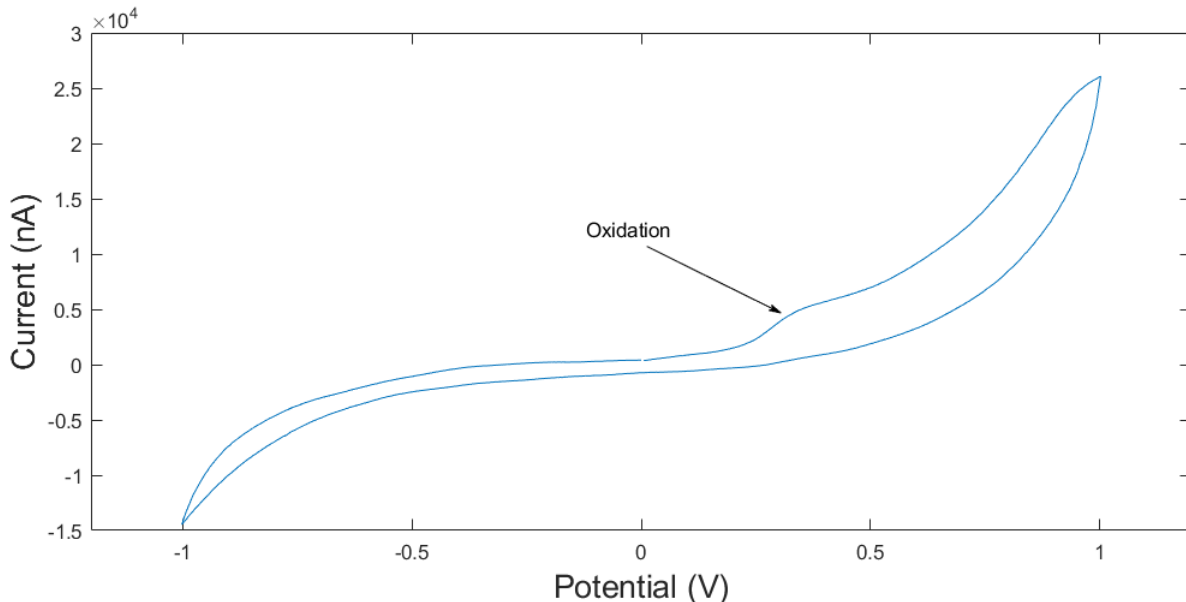


Figure 20: Cyclic Voltammetry at 14 mg/l O₂ concentration, for the Pt-on-BDD electrode

Figure 21 shows the data for stabilized reduction current and for oxygen concentration, plotted over time. The oxygen is increased over time from 0 to 35 mg/l. The graph indicates an increase in current with the increase of oxygen concentration, however there are significant spikes in current, for O₂ levels between 10 and 20 mg/l. To better observe their relationship, the sensor output of reduction current is plotted against the oxygen concentration to obtain a calibration curve as seen in Figure 22. The gradient and intercept with their uncertainties are calculated with MATLAB.

$$\text{gradient} = 271.253 \pm 9.054 \quad (25)$$

$$\text{intercept} = 3105.882 \pm 204.819 \quad (26)$$

The intercept of the best fit line has a significant value of 3105.882 ± 204.819 and it can be interpreted as a background current which causes errors for low oxygen concentrations. The accuracy of the reading is dependent on oxygen levels. For concentrations lower than 20 m/l, the sensor readings have greater errors. However, for higher oxygen concentrations, the background current becomes less significative for the resulting reduction currents and the accuracy of the readings improves. The response time has been calculated to be within one second at 30mg/l. An electrode's sensitivity is given by the gradient of the calibration curve's best fit and it is $271.253 \pm .054$ nA per mg/l of dissolved oxygen. The calibration line equation is arranged to give the signal conversion equation below:

$$\text{Oxygen concentration} = \frac{\text{Reduction current} - 3105.882 \pm 204.819}{271.253 \pm 9.054} \quad (27)$$

The R-squared value is found to be of 0.968, meaning the precision of the correctness of the measurements is lacking in comparison with previous experimental sample. Thus, it becomes clear that although this sample has a better stability over time, its calibration curve is less fit than the one of the Pt-on-diamond microelectrode array.

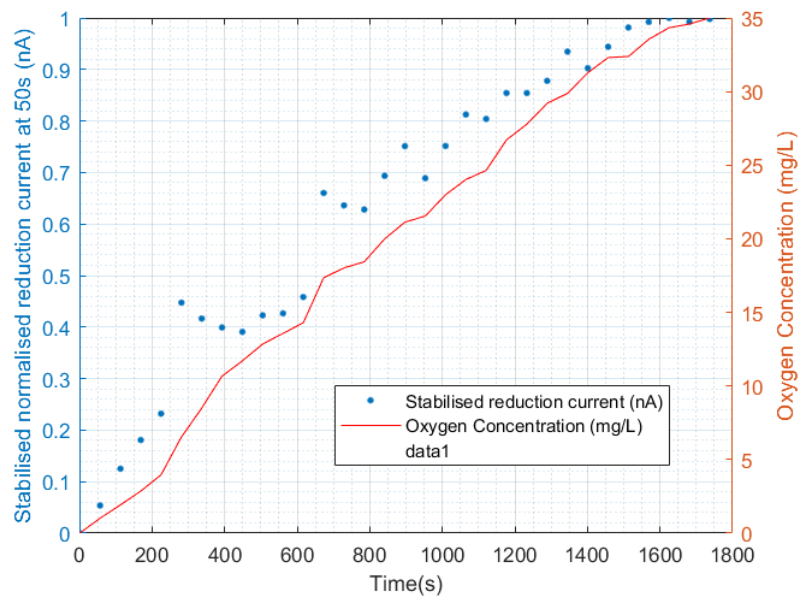


Figure 21: Data for stabilized reduction current and for oxygen concentration, plotted over time, for the 3nm NPs Pt on BDD

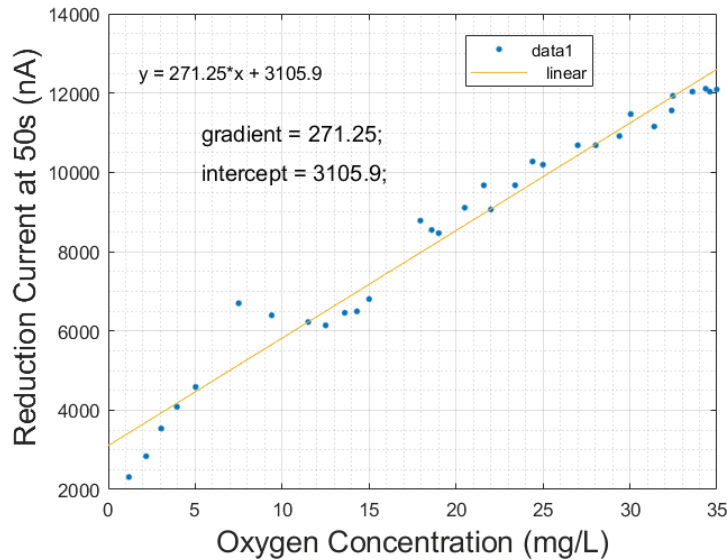


Figure 22: Calibration curve for the 3nm-Pt-on-BDD electrode, for the 3nm NPs Pt on BDD

5.3 Graphitic Microchannel Array (GMC)

The last sample studied is a Graphitic Microchannel (GMC) Array electrode. A cylindrical area of intrinsic diamond was treated by laser, with the surface presenting graphitic material as a product of the cutting. The sp₂ regions are promoting increased electrocatalytic oxygen reduction.

Figure 23 represents the measurement pulse obtained as output current against time. Figure 24 shows the Cottrell plot in which the output current is shown over the inverse square root of time. It is expected that the current deviates higher than predicted by Cottrell in almost all electrode situations. In the GMC's case, it deviates higher owing to the significant involvement of the edge effect. The Cottrell equation is defined for planar electrode mode, which the microchannel array deviates from at high time value.

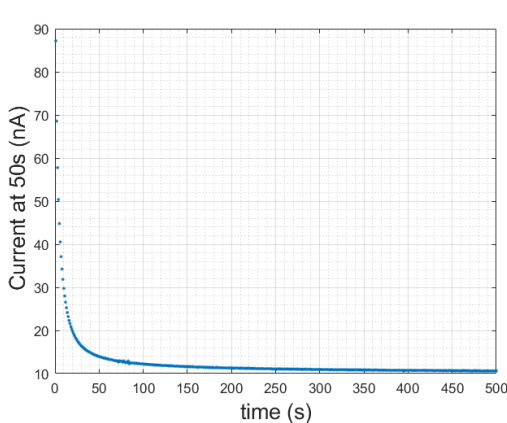


Figure 23: Current against Time for GMC

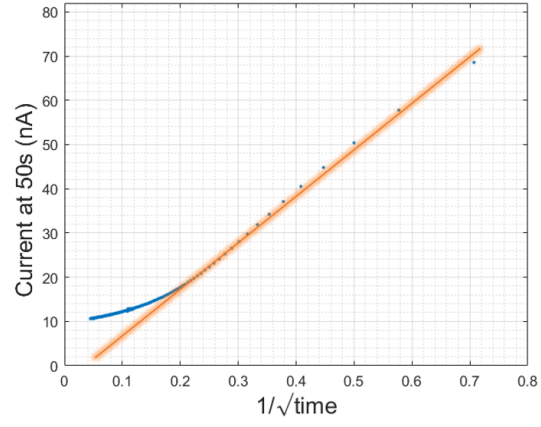


Figure 24: Current against Inverse Square Root of Time for GMC

A continuous measurement for oxygen concentrations up to 20 mg/l has been performed on the GMC. The data for the stabilised reduction current and that for the oxygen concentration from the optical sensor, have been plotted over time, as shown in Figure 25. A strong correlation between the reduction current and the oxygen concentration is observed, to better investigate it the calibration curve is plotted as seen in Figure 26. It is clear that the reduction current values are proportional to the oxygen levels. Even at really small oxygen concentration, the errors are significantly smaller than for previous samples. This is also indicated by the highest R-squared value yet, of 0.995. The starting reduction current is of circa 7 nA, and it's the smallest current between the three samples, this is due to the sample having the smallest surface area.

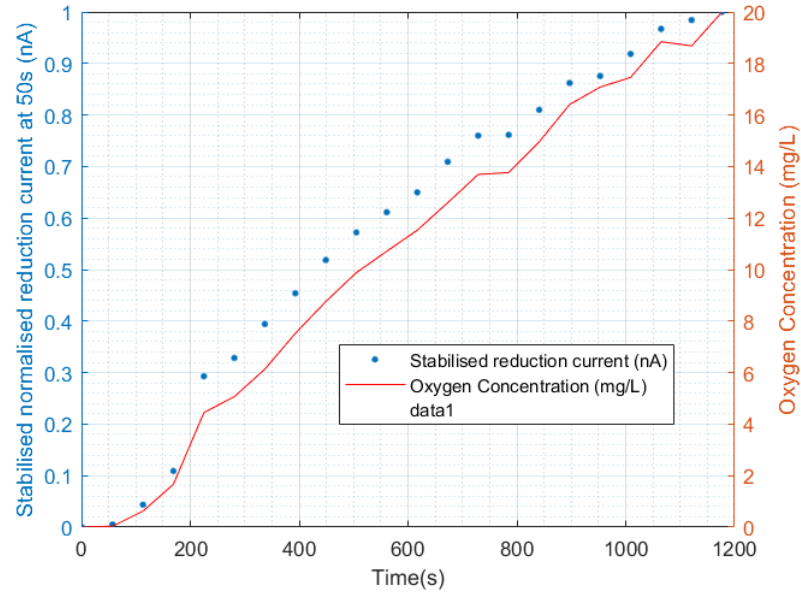


Figure 25: Data for stabilized reduction current and for oxygen concentration, plotted over time, for the GMC

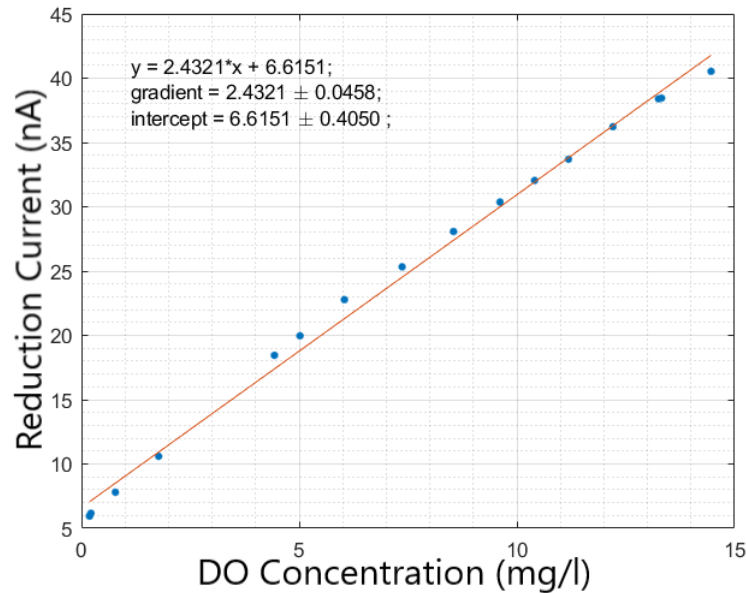


Figure 26: Calibration Curve for the GMC

The gradient and intercept are found with MATLAB and are as follows:

$$\text{gradient} = 2.432 \pm 0.046 \quad (28)$$

$$\text{intercept} = 6.615 \pm 0.405 \quad (29)$$

The calibration line equation is arranged to give the signal conversion

equation below:

$$\text{Oxygen concentration} = \frac{\text{Reduction current} - 6.615 \pm 0.405}{2.432 \pm 0.046} \quad (30)$$

The response time T_{90} is the time it takes the measurement pulse to reach 90% of the steady state current value. At an O₂ concentration of 20mg/l the steady state current is 19.97 nA, and the response time is 8.3 s. The sensitivity of the electrode is 2.432 ± 0.046 nA per mg/l of dissolved oxygen.

5.4 Discussion

Three working electrodes with different fabrication processes of diamonds have been analysed and experimented on. Potential step and cyclic voltammetry procedures were utilised to assess the performance of each. The PtBDD electrode has impressive long-term response stability at constant oxygen concentration. However, the PtDMA and the GMC show a better calibration curve, with the latter having a stronger correlation of reduction current on dissolved oxygen concentration.

Stability over time was determined by examining the drift in the sensor when measuring at a constant oxygen concentration and recording output current over time. Figures 16 and 17 show the first and last 4 measurement pulses for the PtBDD electrode for a testing measurement carried out for 50 minutes. The stabilised reduction current decreased by 1.4 %, which demonstrates better long-term stability than the Pt-on-diamond-disc microelectrode, which had a drift in current of circa 25.62%. The long-term-stability test of the GMC has not yet been examined; thus, it will not be compared in the following explanation.

One of the reasons the PtDMA had worse stability is because it does not function completely in the diffusion-limited regime. Considering the reaction rate to be partly kinetically constrained, then the reaction rate may be impaired by shifts in the solution's pH. Throughout the long-term stability testing, CO_2 could have been dissolved in the DI water solution and contribute to the production of H_2CO_3 . This would dissociate and decrease the pH in the cell. Thus, protons will allow new pathways for oxygen reduction reaction, and the current will increase.

Another explanation why the PtDMA is not as stable is because of the contamination of the sample or of the reference electrode which leads to a faradaic background drift in current over time. When considered these aspects, a full electrode reconditioning was performed before running other experiments. The degradation of the Pt-on-diamond disc microelectrode was expected since it has been used many times for other research purposes in the past few years.

Besides, the fact that PtBDD electrode has better stability over time is also a result of better ohmic contact among Pt and diamond nanoparticles, which is due to the fabrication technique of this device and more importantly, due to the gas phase synthesis process of the Pt NPs.

The plot of a sensor reading vs parameter value gives the calibration curve of that sensor. In this research, the data for the reduction current plotted against the data from the optical oxygen sensor show the calibration curve, as seen in Figure 12, Figure 22 and Figure 26. The data is fit to a linear regression using MATLAB. And by measuring the coefficient of determination, R^2 , the calibration curve is examined. The higher R^2 the better the fit. By this method, it has been experimentally proven that the PtDMA ($R^2 = 0.977$) and the GMC ($R^2=0.991$) have the better calibration curve, meaning they show a stronger correlation of reduction current on dissolved oxygen concentration.

The PtBDD electrode has a coefficient of determination of only 0.967 partly because its background current is significantly larger than for the other two

samples. As it can be observed from Figure 22, the intercept is 3105.9 nA, this can be interpreted as background current, causing large errors for oxygen concentrations lower than 20 mg/l.

Additionally, the better fit to the calibration curve is also due to the complexity and enhanced electrochemical properties of the two devices and proves their suitability as a working electrode in an oxygen sensor. The microdisc array structure has proved to have many advantages, and it is at the base of the design of both the PtDMA and the GMC. The PtDMA has a microdisc array obtained by creating holes in the passivation layer, which has shown to be predisposed to degradation over time. Thus, the GMC is an upgraded version since the microdisc conductive features are created directly on the intrinsic diamond using a laser graphitisation process, without the need of the passivation layer. This technique was proven to be superior, since the GMC is the better indicator of oxygen levels.

Moreover, the GMC's calibration curve can be considered for smaller DO range of 4-14.5 mg/l, since the common range encountered in water monitoring is of 4-7 mg/l. Within this range, the current errors are minimal and the coefficient of correlation (R^2) is increased to 0.999. The sensitivity and liner response range will be 2.2058 ± 0.0221 and $4.432 - 14.32$, respectively. Figure 27 is the Calibration Curve for the GMC, for 4-14 mg/l DO.

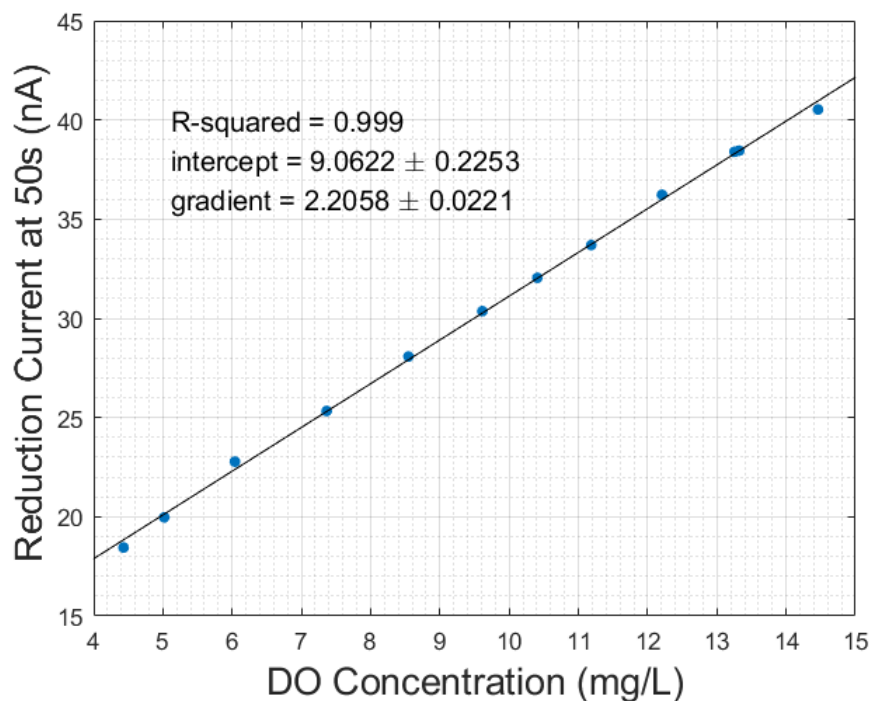


Figure 27: Calibration Curve for the GMC, for DO concentrations f 4-14 mg/l

A comparison is made with polarographic sensors for dissolved oxygen measurements as reported in various research papers. The comparative analysis in Table 2 demonstrates that the proposed electrodes may be used to sensitively monitor the DO levels. The GMC shows the highest coefficient of determination, along with other two reported oxygen sensors from [40] and [41]. Besides, the latter two electrodes are more susceptible to damage and would be unsuited for extreme environment conditions, whereas the GMC is more durable and its fabrication process leaves the diamond intact and able to be utilised at a sealing window for high pressure and temperature devices. The PtDMA had the best detection limit, while the PtBDD had best response time. This was an expected result given the Cottrell Equation from Subsection 3.3.3.1, where it is shown that the surface of the electrode is inversely proportional to the response time. Thus, the electrode with the largest surface area, has the fastest response time.

Experimental Electrode	R^2	Sensitivity	Response Time	Linear Response Range	Detection Limit	Stability	Over time
RuO ₂ electrode [42]	0.9694	0.56 $\mu\text{A} \times \mu\text{M}$	240s	3-11mg/l	-	-	
Hemin-Based Electrode [43]	0.9872	8.5 $\mu\text{A} / (\text{mg/l})$	200s	2-7 mg/l	-	Circa 3% drift in current	
Nickel-Salen Polymeric film modified electrode [44]	0.9976	3.54 \pm 0.978 $\mu\text{A} / (\text{mg/l})$	-	3.95-9.20 mg/l	0.71 mg/l	-	
RGO/Ag nanocomposite modified GCE [45]	0.991	0.205 $\mu\text{A} \times \mu\text{M}$	<5s	0-120 μM	0.031 μM	-	
Fluorinated diamond micro-electrodes [46]	0.9988	0.142 \pm 0.004 nA $\times \mu\text{M}$	<1s	0-273.75 μM	0.63 μM	-	
CDSH /FeTM-PuP/ CD-SHAuNp Modified Gold Electrode [40]	0.999	5.5 $\mu\text{A} / (\text{mg/l})$	1s	0.2-6.6 mg/l	0.02 mg/l	Great stability	1
GC electrodes modified with CoTSPc/PLL film [41]	0.999	11.0 $\mu\text{A} / (\text{mg/l})$	-	0.2-8.0mg/l	96 $\mu\text{g/l}$	4.5% drift in current	
Pt-on-diamond microelectrode array	0.977	3.479 \pm 0.057 nA per mg/l	4.9s	0-35mg/l	0.011 mg/l	25.62%	
3nm Pt on BDD electrode	0.968	271.253 \pm 9.054 nA per mg/l	<1s	0-35mg/l	2.17 mg/l	1.4%	
GMC electrode	0.999	2.432 \pm 0.046 nA per mg/l	8.3s	4.43-14.3 mg/l	0.185 mg/l	-	

Table 2: Comparison Table for Oxygen Sensors

Although all three electrodes could be added in the design of an oxygen sensor, the GMC electrode demonstrates a good current-to-oxygen correlation, great detection limit and has better response time than other electrodes from the table reported in Article [43], and Article [42]. Overall, it has been found to have satisfactory characteristics in all metrics. Moreover, although reported sensors from [40] and [41] have same excellent coefficient of determination as the GMC, their working electrodes would not be suitable for

harsh environmental conditions. The GMC's microdisc conductive features are created directly on the intrinsic diamond using a laser graphitisation process, thus the use of a passivation layer is avoided. The intrinsic diamond remains intact and may be applied as a sealing window for extreme temperature and pressure systems. Thus, the Ag/AgCl reference electrode, along with the Pt foil counter electrode and the GMC is the 3-electrode-sensor design that demonstrated the most impressive performance as DO sensor for real-time measurements.

5.5 Design Concept

This section presents the design concept of an oxygen sensor for extreme environments, in particular for submarines. The ocean provides some of the hardest conditions for military electronics equipment. Thus, this must address high-temperature and high-pressure situations, plus the added stressors of seawater corrosion, and numerous forms of shock.

A design concept for the oxygen sensor as seen in Figures 28 and 29 is built in Blender. The design shows the connecting wires, covered in a protective shield braid, followed by an anti-shock and insulation jacket. To ensure that the sensor is easily mounted on the submarine, a stainless steel thread will cover the case of the connector. As a result, the oxygen sensor can be screwed onto the vessel's surface panel to ensure a quick fit and easy unscrewing when cleaning or calibration is required. Stainless Steel is a material highly resistant to corrosion. The rubber-O rings support an elastic collision.

For the reasons set out in chapter 3.2.3, a three-electrode system was chosen. This device includes a reference electrode, a Pt counter electrode and a GMC working electrode. The GMC is the ideal choice due to its excellent durability and ability to overcome temperature cycles and pressures of up to 600 GPa (as presented in 3.4). Furthermore, since the GMC manufacturing process keeps the diamond intact, the electrode used as a sealing window for its compartment will not cause any leakage. The three-electrode cell is screwed onto the rest of the oxygen sensor by means of a stainless steel hex nut. Hence, through this method, the parts of the sensor can be quickly assembled and disassembled when fixing is needed. Figures 31 and 30 are additional figures to present the design of the oxygen sensor.

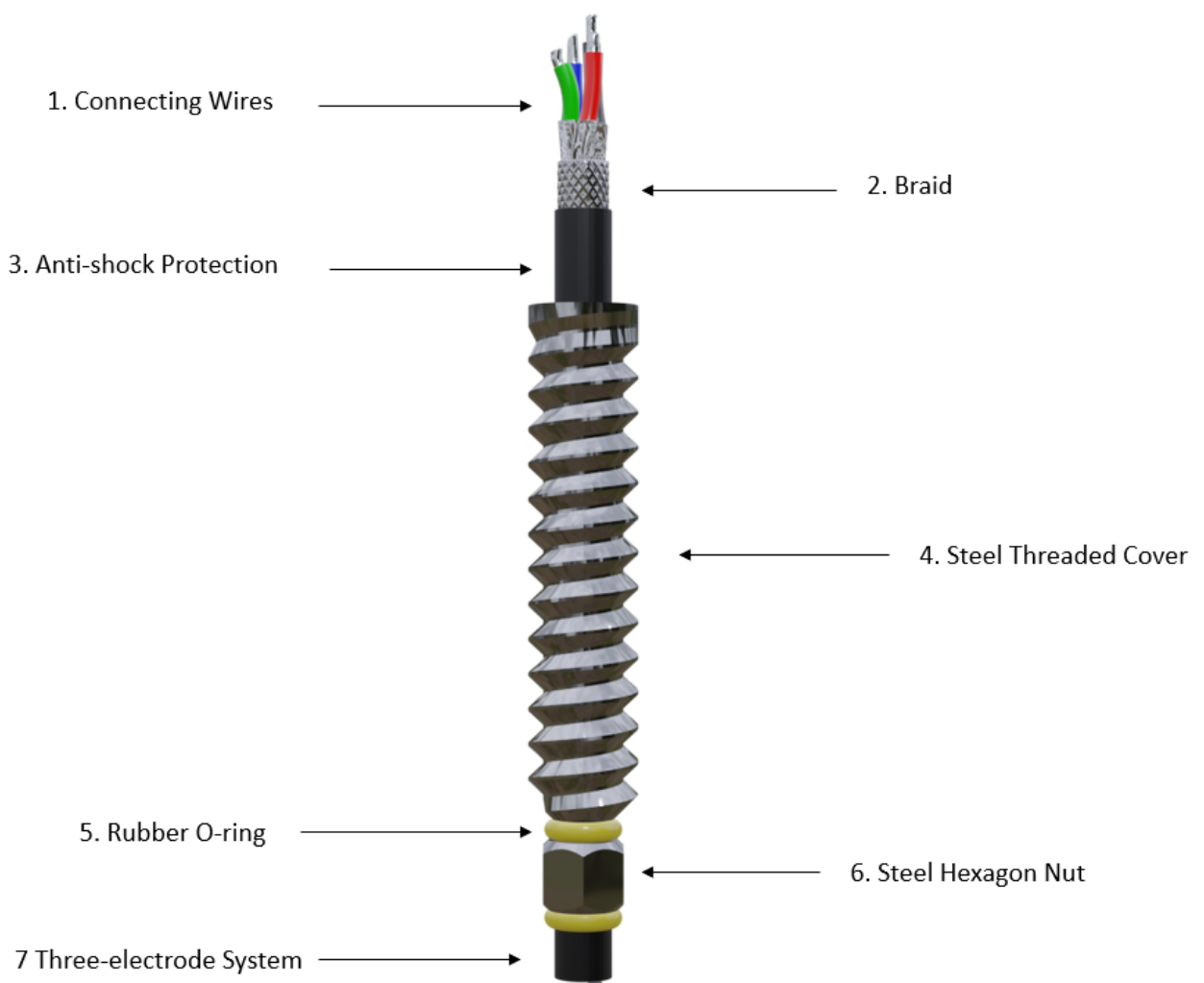


Figure 28: Oxygen Sensor for Extreme Environments

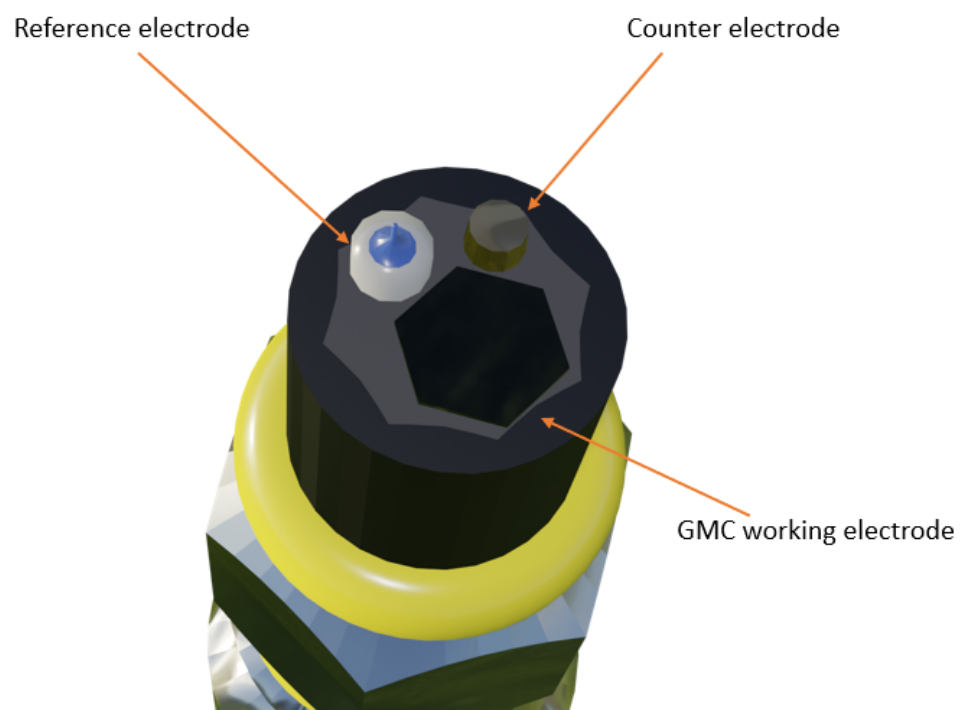


Figure 29: 3-Electrode System



Figure 30: Concept of Oxygen Sensor in water

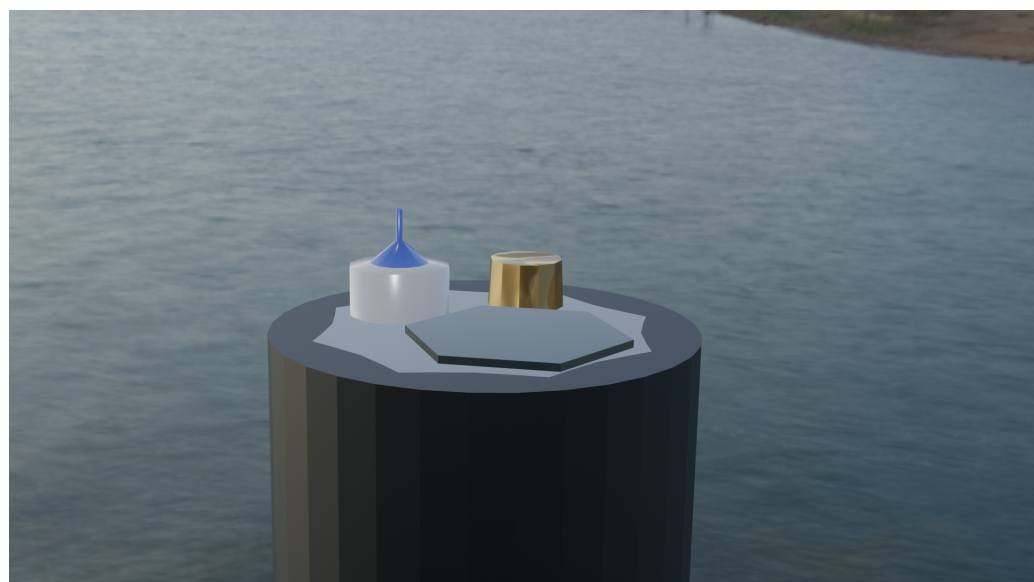


Figure 31: Concept of the three-electrode cell

6 Conclusion

In conclusion, the goals of this project have been accomplished, and three diamond-based samples were demonstrated as working electrodes for an amperometric oxygen sensor. The excellent sensitivity, stability and rapid response time of the electrodes make them perfect for measuring DO in real-time. In addition, the durability of the diamonds and the fabrication technique of the samples permit them to undergo harsh environmental conditions. The use of Graphitic Microchannel Array electrode in an oxygen sensor has been demonstrated for the first time. Its initial results are both impressive and promising and prove it a suitable option for oxygen sensors for extreme environment applications.

The sensing characteristics of the three experimental electrodes were compared with those of other seven amperometric oxygen sensors, with metrics as stated in their respective research papers. The comparative study shows that the proposed electrodes can be used to sensitively track the DO levels, each performing better in different areas. The PtBDD electrode has impressive long-term response stability with a current drift of only 1.4% at constant oxygen concentration. In contrast, the PtDMA has a drift of approximately 21.42%. The excellent stability of the PtBDD may indicate a better ohmic contact among Pt and diamond nanoparticles, which is due to the fabrication technique of this device and more importantly, because of the gas phase synthesis process of the Pt NPs. The Pt-on-diamond microelectrode array ($R^2=0.977$) and the GMC ($R^2=0.999$) show a stronger correlation of reduction current on oxygen concentration. The microdisc array proved to have many advantages and is at the basis of the design of both the PtDMA and the GMC. The PtDMA has a microdisc array obtained by creating holes in the passivation layer that are predisposed to degradation over time. The GMC is, therefore, an improved version, because the microdisc conductive features are directly formed by means of laser graphitisation, avoiding the use of a passivation layer.

Compared to the other two experimental electrodes, the GMC demonstrated to have better accuracy in results and performed well in every experiment. Its detection limit and response time were found to be 0.185mg/l, and 8.3s, respectively. Creating microchannels directly on the diamond through laser graphitisation resulted in reliable and replicable results. A design concept for an oxygen sensor for submarine applications was built in Blender. It includes the GMC as its working electrode.

For future work, it is beneficial to analyze whether there are any variations in output current while performing chronoamperometry at lower temperatures. This finding would be useful given that real-time applications under extreme conditions usually tackle severe temperature cyclings. In addition, further research on the GMC will determine whether it can be used as a multi-purpose working electrode for real-time metrics.

References

- [1] C. C. of Ministers of the Environment, "Canadian water quality guidelines for the protection of aquatic life:dissolved oxygen (freshwater)," *Canadian environmental quality guidelines*, 1999.
- [2] A. Azevedo and N. Ferreira, "Nanodiamond films for applications in electrochemical systems and aeronautics and space technology," *Química Nova*, vol. 29, pp. 129–136, 02 2006.
- [3] T. Rao, T. A. Ivandini, C. Terashima, B. Sarada, and A. Fujishima, "Applications of bare and modified diamond electrodes in electroanalysis," *New Diamond and Frontier Carbon Technology*, vol. 13, pp. 79–88, 01 2003.
- [4] M. Schwartz, "Polarographic oxygen sensors," *Journal of Clinical Engineering*, 1978.
- [5] E. Gnaiger, *Polarographic Oxygen Sensors, the Oxygraph, and High-Resolution Respirometry to Assess Mitochondrial Function*, 01 2008, pp. 325 – 352.
- [6] M. Sosna, G. Denuault, R. W. Pascal, R. D. Prien, and M. Mowlem, "Development of a reliable microelectrode dissolved oxygen sensor," *Sensors and Actuators B: Chemical*, vol. 123, no. 1, pp. 344 – 351, 2007.
- [7] L. Hutton, M. Newton, P. Unwin, and J. Macpherson, "Amperometric oxygen sensor based on a platinum nanoparticle-modified polycrystalline boron doped diamond disk electrode," *Analytical chemistry*, vol. 81, pp. 1023–32, 02 2009.
- [8] T. A. Ivandini, E. Saepudin, H. Wardah, H. Harmesa, N. Dewangga, and Y. Einaga, "Development of a bod sensor using gold-modified boron doped diamond electrodes." *Analytical chemistry*, vol. 84, 10 2012.
- [9] M. De Feudis, A. Caricato, A. Taurino, P. Ossi, C. Castiglioni, L. Brambilla, G. Maruccio, A. G. Monteduro, E. Broitman, G. Chiodin, and M. Martino, "Diamond graphitization by laser-writing for all-carbon detector applications," *Diamond and Related Materials*, vol. 75, 12 2016.
- [10] R. Moors, *Diamond and sp₂ carbon for green energy applications*, 2019.
- [11] "Sp₃ hybridization," 12 2016.
- [12] M. N. R. Ashfold, P. W. May, C. A. Rego, and N. M. Everitt, "Thin film diamond by chemical vapour deposition methods," *Chem. Soc. Rev.*, vol. 23, pp. 21–30, 1994. [Online]. Available: <http://dx.doi.org/10.1039/CS9942300021>
- [13] F. P. Bundy, H. T. Hall, H. M. Strong, and R. H. Wentorf, "Man-Made Diamonds," , vol. 176, no. 4471, pp. 51–55, Jul. 1955.
- [14] J. C. Angus.
- [15] C. J. Wort and R. S. Balmer, "Diamond as an electronic material," *Materials Today*, vol. 11, no. 1, pp. 22 – 28, 2008.
- [16] R. Kalish, "Doping of diamond," *Carbon*, vol. 37, 1999.
- [17] M. Brehob, R. Enbody, Y.-K. Kwon, and D. Tomanek, "The potential of carbon-based memory systems," 02 1999, pp. 110 – 114.
- [18] Y. A. D. L. D. L. W. W. Q. Wei, Y.; Jiao.
- [19] J. Yang, Z. Wang, Y. Li, Q. Zhuang, and J. Gu, "Real-time monitoring of dissolved oxygen with inherent oxygen-sensitive centers in metal-organic frameworks," *Chemistry of Materials*, vol. 28, no. 8, pp. 2652–2658, 2016.

- [20] L. Yan, Z. Chen, Z. Zhang, C. Qu, L. Chen, and D. Shen, "Fluorescent sensing of mercury(ii) based on formation of catalytic gold nanoparticles," *Analyst*, pp. 4280–4283, 2013.
- [21] P. Oomen, "Small systems, small sensors: Integrating sensing technologies into microfluidic and organ-on-a-chip devices," Ph.D. dissertation, University of Groningen, 2016.
- [22] I. Helm, L. Jalukse, and I. Leito, "Measurement uncertainty estimation in amperometric sensors: A tutorial review," *Sensors (Basel, Switzerland)*, vol. 10, pp. 4430–55, 05 2010.
- [23] A. Paul, T. Laurila, V. Vuorinen, and S. V. Divinski, *Fick's Laws of Diffusion*. Springer International Publishing, 2014, pp. 115–139.
- [24] P. J. Lingane, "Chronopotentiometry and chronoamperometry with unshielded planar electrodes." *Analytical Chemistry*, vol. 36, no. 9, pp. 1723–1726, 1964.
- [25] K. Aoki and J. Osteryoung, "Formulation of the diffusion-controlled current at very small stationary disk electrodes."
- [26] J. L. by I. Montenegro, M. Arlete Queirós, *Microelectrodes: Theory and Applications*. Springer International Publishing, 1990, pp. 5–10.
- [27] O. V. Klymenko, C. Amatore, and I. Svir, "Time-dependent diffusion-migration at cylindrical and spherical microelectrodes: Steady- and quasi-steady-state analytical solution can be used under transient conditions," *Analytical Chemistry*, vol. 79, no. 16, pp. 6341–6347, 2007, pMID: 17637041.
- [28] C. Amatore, A. Oleinick, and I. Svir, "Theoretical analysis of microscopic ohmic drop effects on steady-state and transient voltammetry at the disk microelectrode: A quasi-conformal mapping modeling and simulation," *Analytical Chemistry*, vol. 80, no. 21, pp. 7947–7956, 2008, pMID: 18826243.
- [29] K. B. Oldham and C. G. Zoski, "Comparison of voltammetric steady states at hemispherical and disc microelectrodes," *Journal of Electroanalytical Chemistry and Interfacial Electrochemistry*, 1988.
- [30] H. Germanischer Lloyd Aktiengesellschaft, *Naval Ship Technology*, 2008.
- [31] P. T. Kissinger and W. R. Heineman, "Cyclic voltammetry," *Journal of Chemical Education*, vol. 60, no. 9, p. 702, 1983.
- [32] A. Q. (UCD). Cyclic Voltammetry .
- [33] *Potentiometry*. John Wiley Sons, Ltd, ch. 5, pp. 165–200.
- [34] X. Chen, F. Wang, Y. Xu, and S. Hu, "A novel amperometric nitric oxide sensor based on polythionine/nafion modified glassy carbon electrode," *Chinese Chemical Letters*, vol. 17, pp. 496–498, 04 2006.
- [35] H.-q. Y. . J.-t. L. Jing, Y., "Study on response time of spe carbon monoxide sensor," *Nat. Sci.*
- [36] L. Jalukse and I. Leito, "Model-based measurement uncertainty estimation in amperometric dissolved oxygen concentration measurement," *Measurement Science and Technology*, vol. 18, p. 1877, 05 2007.
- [37] Z. Qin, P.-N. Wang, and Y. Wang, "Enhanced sensing performance of the amperometric gas sensor by laser-patterning of the polymer membrane electrode," *Sensors and Actuators B-chemical - SENSOR ACTUATOR B-CHEM*, vol. 107, pp. 805–811, 06 2005.

- [38] J. R. Stetter and J. Li, "Amperometric gas sensors a review," *Chemical Reviews*, vol. 108, no. 2, pp. 352–366, 2008, pMID: 18201108.
- [39] D. Ammann, *Ion-Selective Microelectrodes: Principles, Design and Application*. Springer International Publishing, 1985, pp. 230–234.
- [40] F. Damos, R. Luz, A. Tanaka, and L. Kubota, "Dissolved oxygen amperometric sensor based on layer-by-layer assembly using host-guest supramolecular interactions," *Analytica chimica acta*, vol. 664, pp. 144–50, 04 2010.
- [41] R. Luz, F. Damos, A. Tanaka, and L. Kubota, "Dissolved oxygen sensor based on cobalt tetrasulphonated phthalocyanine immobilized in poly-l-lysine film onto glassy carbon electrode," *Sensors and Actuators B: Chemical*, vol. 114, pp. 1019–1027, 04 2006.
- [42] G. Wiranto, S. Widodo, I. D. P. Hermida, R. Manurung, G. Sugandi, Z. Arifin, and W. Wiendartun, "Design and fabrication of thick film dissolved oxygen sensor based on ruo₂ working electrodes for water quality monitoring," *Materials Science Forum*, vol. 917, pp. 59–63, 03 2018.
- [43] L. Hsu, P. Selvaganapathy, J. Brash, Q. Fang, C.-Q. Xu, M. Deen, and H. Chen, "Development of a low-cost hemin-based dissolved oxygen sensor with anti-biofouling coating for water monitoring," *Sensors Journal, IEEE*, vol. 14, pp. 3400–3407, 10 2014.
- [44] C. Martin, T. Dadamos, and M. Teixeira, "Development of an electrochemical sensor for determination of dissolved oxygen by nickel-salen polymeric film modified electrode," *Sensors and Actuators B: Chemical*, vol. 175, p. 111–117, 12 2012.
- [45] L. Fu, Y. Zheng, Z. Fu, A. Wang, and W. Cai, "Dissolved oxygen detection by galvanic displacement-induced graphene/silver nanocomposite," *Bulletin of Materials Science*, vol. 38, 06 2015.
- [46] E. Silva, A. C. Bastos, M. Neto, A. Fernandes, R. Silva, M. Ferreira, M. Zheludkevich, and F. Oliveira, "New fluorinated diamond microelectrodes for localized detection of dissolved oxygen," *Sensors and Actuators B Chemical*, vol. 204, pp. 544–551, 12 2014.